LETTER

https://doi.org/10.1038/s41586-019-1456-0

CD24 signalling through macrophage Siglec-10 is a target for cancer immunotherapy

Amira A. Barkal[1,2,3,4], Rachel E. Brewer[1,2,3], Maxim Markovic[1,2,3], Mark Kowarsky[5], Sammy A. Barkal[1], Balyn W. Zaro[1,2,3], Venkatesh Krishnan[6], Jason Hatakeyama[1,7], Oliver Dorigo[6], Layla J. Barkal[8] & Irving L. Weissman[1,2,3,9]*

Ovarian cancer and triple-negative breast cancer are among the most lethal diseases affecting women, with few targeted therapies and high rates of metastasis. Cancer cells are capable of evading clearance by macrophages through the overexpression of anti-phagocytic surface proteins called 'don't eat me' signals—including CD47[1], programmed cell death ligand 1 (PD-L1)[2] and the beta-2 microglobulin subunit of the major histocompatibility class I complex (B2M)[3]. Monoclonal antibodies that antagonize the interaction of 'don't eat me' signals with their macrophage-expressed receptors have demonstrated therapeutic potential in several cancers[4,5]. However, variability in the magnitude and durability of the response to these agents has suggested the presence of additional, as yet unknown 'don't eat me' signals. Here we show that CD24 can be the dominant innate immune checkpoint in ovarian cancer and breast cancer, and is a promising target for cancer immunotherapy. We demonstrate a role for tumour-expressed CD24 in promoting immune evasion through its interaction with the inhibitory receptor sialic-acid-binding Ig-like lectin 10 (Siglec-10), which is expressed by tumour-associated macrophages. We find that many tumours overexpress CD24 and that tumour-associated macrophages express high levels of Siglec-10. Genetic ablation of either CD24 or Siglec-10, as well as blockade of the CD24–Siglec-10 interaction using monoclonal antibodies, robustly augment the phagocytosis of all CD24-expressing human tumours that we tested. Genetic ablation and therapeutic blockade of CD24 resulted in a macrophage-dependent reduction of tumour growth in vivo and an increase in survival time. These data reveal CD24 as a highly expressed, anti-phagocytic signal in several cancers and demonstrate the therapeutic potential for CD24 blockade in cancer immunotherapy.

CD24, also known as heat stable antigen or small-cell lung carcinoma cluster 4 antigen, is a heavily glycosylated glycosylphosphatidylinositol-anchored surface protein[6,7]. It is known to interact with Siglec-10 on innate immune cells to dampen damaging inflammatory responses to infection[8], sepsis[9], liver damage[10] and chronic graft versus host disease[11]. The binding of CD24 to Siglec-10 elicits an inhibitory signalling cascade, which is mediated by Src homology region 2 domain-containing phosphatases, SHP-1 and/or SHP-2. These phosphatases are associated with the two immunoreceptor tyrosine-based inhibition motifs in the cytoplasmic tail of Siglec-10, thereby blocking Toll-like-receptor-mediated inflammation and the cytoskeletal rearrangement required for cellular engulfment by macrophages[12–14]. Studies have shown that CD24 is expressed by several solid tumours[15,16]; however, a role for CD24 in modulating tumour immune responses has not yet been shown. We therefore sought to investigate whether CD24-mediated inhibition of the innate immune system could be harnessed by cancer cells as a mechanism of avoiding clearance by macrophages that express Siglec-10.

To assess the role of CD24–Siglec-10 signalling in regulating the macrophage-mediated immune response to cancer, we examined the expression of CD24 and Siglec-10 in various tumours and associated immune cells. RNA-sequencing data from The Cancer Genome Atlas (TCGA) and the Therapeutically Applicable Research to Generate Effective Treatment Program (TARGET) revealed high expression of *CD24* in nearly all tumours analysed (Extended Data Fig. 1a), as well as broad upregulation of *CD24* expression in several tumours as compared to known innate immune checkpoints (Fig. 1a). The largest upregulation of *CD24*—a $\log_2$ fold increase of more than nine—was observed in ovarian cancer; in addition, *CD24* expression was significantly higher in triple-negative breast cancer (TNBC) than in healthy breast cells or in oestrogen- and progesterone-receptor-positive (ER^+PR^+) breast cancers (Extended Data Fig. 1b, c). Stratification of patients by *CD24* expression revealed increased relapse-free survival for patients with ovarian cancer and an overall survival advantage for patients with breast cancer with lower *CD24* expression (Fig. 1b, c). We investigated *CD24* and *SIGLEC10* expression at a cellular level within the tumour by using single-cell RNA-sequencing data from six primary samples of TNBC[17] (NCBI Sequence Read Archive: PRJNA485423; Fig. 1d, Extended Data Fig. 1d, e). TNBC cells exhibited robust expression of *CD24*, whereas its expression was weak in all other cell clusters, thus illustrating the potential of CD24 as a tumour-specific marker (Fig. 1d). A substantial fraction of tumour-associated macrophages (TAMs) were found to express *SIGLEC10*, indicating the possibility of CD24–Siglec-10 interactions in TNBC (Fig. 1d). *CD24* expression was substantially higher than *PD-L1* (also known as *CD274*) expression in all patients analysed (Extended Data Fig. 1f), whereas *CD47* was highly expressed by all cell types (Fig. 1d). Fluorescence-activated cell sorting (FACS) analyses of primary human tumours revealed robust expression of the CD24 protein in breast cancer cells and ovarian cancer cells, and TAMs from both tumour types were found to express Siglec-10 (Fig. 1e, f, Extended Data Fig. 2a). Human peritoneal macrophages obtained from patients without cancer expressed low levels of Siglec-10 (Extended Data Fig. 2b). Analysis of subsets of peripheral blood mononuclear cells revealed low expression of Siglec-10 and CD24 in T cells, natural killer cells and monocytes, whereas B cells were found to express modest levels of Siglec-10 and high levels of CD24 (Extended Data Fig. 2c, d).

To investigate a role for CD24–Siglec-10 signalling in regulating the macrophage-mediated anti-tumour immune response (Fig. 2a), we engineered a polyclonal subline of the normally CD24-positive MCF-7 human breast cancer cell line that was deficient in CD24 (ΔCD24). Although unstimulated (M0) human donor-derived macrophages expressed low levels of Siglec-10 as measured by FACS, the addition of two inhibitory cytokines—TGFβ1 and IL-10—induced robust expression of Siglec-10, indicating that Siglec-10 expression may be regulated by TAM-specific gene-expression programs[18] (Extended Data Fig. 2e). Macrophages stimulated by TGFβ1 and IL-10 (M2-like)

[1]Institute for Stem Cell Biology and Regenerative Medicine, Stanford University School of Medicine, Stanford, CA, USA. [2]Ludwig Center for Cancer Stem Cell Research and Medicine, Stanford University School of Medicine, Stanford, CA, USA. [3]Stanford Cancer Institute, Stanford University School of Medicine, Stanford, CA, USA. [4]Stanford Medical Scientist Training Program, Stanford University, Stanford, CA, USA. [5]Department of Physics, Stanford University, Stanford, CA, USA. [6]Department of Obstetrics and Gynecology, Division of Gynecologic Oncology, Stanford University School of Medicine, Stanford, CA, USA. [7]Department of Urology, Stanford University School of Medicine, Stanford, CA, USA. [8]Department of Medicine, Stanford University School of Medicine, Stanford, CA, USA. [9]Department of Pathology, Stanford University School of Medicine, Stanford, CA, USA. *e-mail: irv@stanford.edu

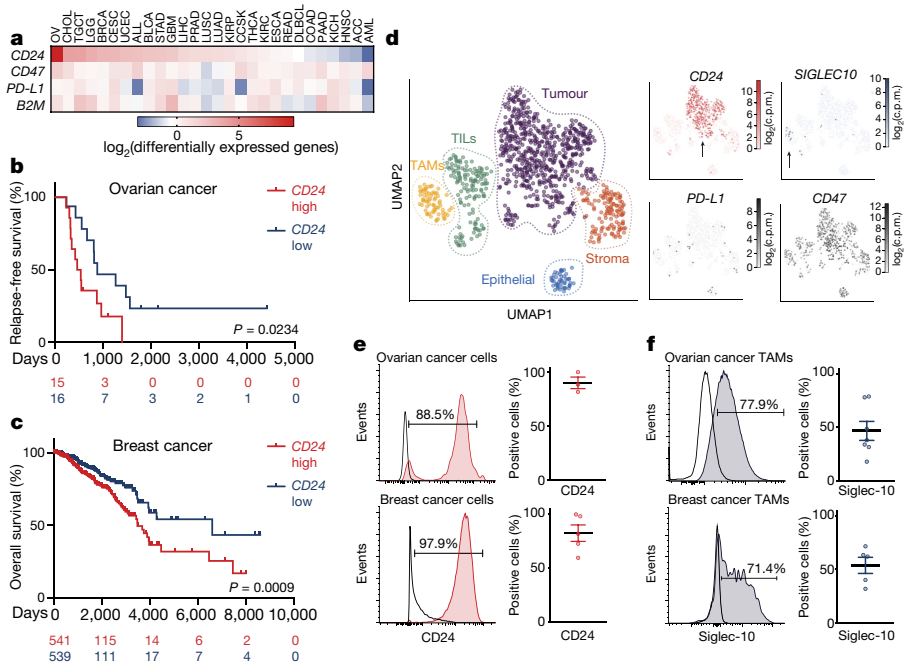

Fig. 1 | CD24 is overexpressed by human cancers and is co-expressed with Siglec-10 on TAMs. a, Heat map of *CD24* tumour to matched normal expression ratios ($\log_2$(differentially expressed genes)) compared to known immune checkpoints. Tumour study abbreviations and *n* values are provided in Supplementary Table 1. **b**, **c**, Relapse-free survival of patients with ovarian cancer ($n = 31$) (**b**) and overall survival of patients with breast cancer ($n = 1{,}080$) (**c**) with high or low *CD24* expression as defined by the median. Two-sided *P* value computed by a log-rank (Mantel–Cox) test. Numbers of subjects at risk in the high group (red) compared with the low group (blue) are indicated below the *x* axes. **d**, Uniform manifold approximation and projection (UMAP) dimension 1 and 2 plots displaying TNBC cells from 6 patients ($n = 1{,}001$ single cells). Left, cells are coloured by cluster identity; right, *CD24* (red) and *SIGLEC10* (blue) expression overlaid onto UMAP space as compared to the expression of *CD47* (grey) and *PD-L1* (grey). **e**, Left, representative histogram (obtained from flow cytometry results) of CD24 expression by ovarian cancer cells (top) or breast cancer cells (bottom); right, frequency of $CD24^+$ cancer cells in ovarian cancer ($n = 3$ donors) (top) or breast cancer ($n = 5$ donors) (bottom). Data are mean ± s.e.m. **f**, Left, representative histogram measuring the expression of Siglec-10 by ovarian cancer TAMs (top) or breast cancer TAMs (bottom); right, frequency of Siglec-10^+ TAMs in ovarian cancer ($n = 6$ donors) (top) or breast cancer ($n = 5$ donors) (bottom). Data are mean ± s.e.m.

were less phagocytic than unstimulated macrophages at baseline levels (Extended Data Fig. 2f). We found that stimulation with the classic M2-polarizing cytokine IL-4 was also sufficient to induce Siglec-10 expression (Extended Data Fig. 2g). Co-culture of either wild-type or ΔCD24 cells with M2-like macrophages expressing Siglec-10 revealed that *CD24* genetic deletion alone was sufficient to potentiate phagocytosis (Fig. 2b). ΔCD24 cells were also significantly more sensitive to CD47 blockade (using Clone 5F9-G4[19]) than were wild-type cells, suggesting the cooperativity of combinatorial blockade of CD24 and CD47. To measure phagocytic clearance by automated live-cell microscopy, GFP^+ wild-type and ΔCD24 cells were labelled with the pH-sensitive dye pHrodo Red[20] and were co-cultured with macrophages. Over the course of 36 h, we found that ΔCD24 cells were more readily engulfed and degraded in the low-pH phagolysosome, as compared with wild-type cells (Fig. 2c).

The blockade of Siglec-10 using monoclonal antibodies augmented the phagocytic ability of macrophages, thereby confirming a role for Siglec-10 in inhibiting phagocytosis (Fig. 2d). To further investigate the effect of Siglec-10 expression on phagocytosis, we knocked out the *SIGLEC10* gene in donor-derived macrophages. Three days after electroporation with a single-guide RNA targeting the *SIGLEC10* locus, we observed a marked reduction in Siglec-10 expression relative to cells electroporated with Cas9 alone (Cas9 control) (Fig. 2e). *SIGLEC10* knockout macrophages demonstrated significantly greater phagocytic ability than Cas9 control macrophages (Fig. 2f).

Siglec-10 has been reported to interact with the highly sialylated form of CD24[13,14]. Accordingly, we observed that binding of Siglec-10–Fc (Fc, crystallizable fragment) to MCF-7 cells was considerably reduced upon surface desialylation (Fig. 2g, Extended Data Fig. 3b). This suggests that Siglec-10 has the capacity to recognize both protein and sialic acid ligands, and therefore probably has varied ligands that extend beyond CD24. Indeed, we observed that *CD24* deletion alone is insufficient to completely abrogate Siglec-10–Fc binding in the presence of surface sialylation (Extended Data Fig. 3a, b). However, in the absence of surface sialylation, Siglec-10–Fc binding was nearly abolished by *CD24* deletion, suggesting that CD24 is the primary protein ligand for Siglec-10 (Fig. 2h, Extended Data Fig. 3b). We found that desialylation did not reduce the enhancement of phagocytosis that was observed upon *CD24* deletion, indicating that CD24 sialylation is not required to inhibit phagocytosis (Extended Data Fig. 3c). Neither recombinant Siglec-5–Fc nor Siglec-9–Fc were found to bind $CD24^+$ MCF-7 cells, although both were highly expressed by donor-derived macrophages (Extended Data Fig. 3d–g).

To investigate the human therapeutic potential of these findings, we examined whether direct monoclonal antibody (mAb) blockade of CD24 could enhance the phagocytosis of $CD24^+$ human cancers by disrupting CD24–Siglec-10 signalling (Extended Data Fig. 4a). Automated live-cell microscopy revealed that MCF-7 pHRodo Red^+ cells treated with a CD24-blocking mAb (clone SN3)[21] were more readily engulfed into the low pH phagolysosome, as demonstrated by an enhanced red signal over time (Fig. 2i, Extended Data Fig. 4b). Substantial whole-cell phagocytosis was observed by confocal microscopy upon treatment with anti-CD24 mAb, and dual blockade of both CD24 and CD47 further augmented cellular engulfment (Extended Data Fig. 4c, d). Similarly, FACS-based measurements revealed a robust increase in phagocytosis upon the addition of anti-CD24 mAb as compared to the IgG control, which was greater than the effect observed with CD47 blockade (Fig. 3a; the gating strategy for in vitro phagocytosis is shown in Extended Data Fig. 5a). The response to anti-CD24 mAb was found to be dose-dependent and saturable (Extended Data Fig. 5b). CD24 blockade augmented the phagocytosis of all CD24-expressing cancer cell lines tested—including breast cancer (MCF-7), pancreatic

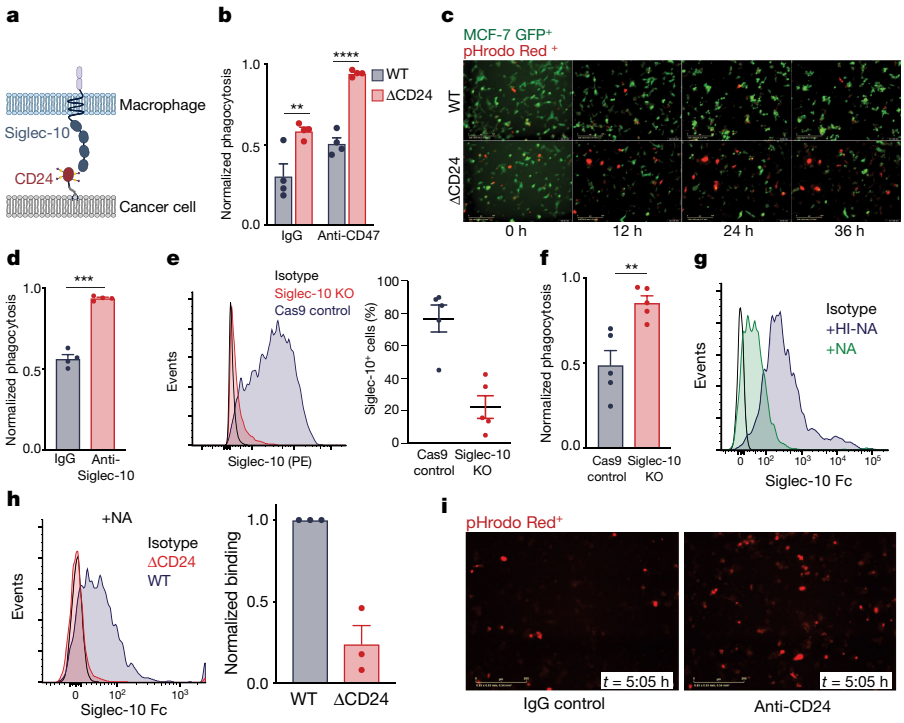

Fig. 2 | CD24 directly protects cancer cells from phagocytosis by macrophages. a, Schematic depicting interactions between macrophage-expressed Siglec-10 and CD24 expressed by cancer cells. **b**, Phagocytosis of $CD24^+$ MCF-7 cells (wild-type, WT) and $CD24^-$ (ΔCD24) MCF-7 cells, in the presence or absence of anti-CD47 mAb ($n = 4$ donors; two-way ANOVA with multiple comparisons correction, cell line $F_{(1,12)} = 65.65$; treatment $F_{(1,12)} = 40.30$, $^{**}P = 0.0045$, $^{****}P < 0.0001$). **c**, Representative phagocytosis images of pHrodo Red^+GFP^+ MCF-7 cells (wild-type, top; ΔCD24, bottom) over time; images are representative of two donors. **d**, Phagocytosis of wild-type MCF-7 cells, in the presence of anti-Siglec-10 mAb or IgG control ($n = 4$ donors; paired, two-tailed Student's *t*-test, $^{***}P = 0.0010$). **e**, Left, FACS-based measurement of Siglec-10 expression (phycoerythrin (PE)-conjugated) by Siglec-10 knockout (KO) macrophages (red) compared with Cas9 control (blue); right, frequency of Siglec-10^+ macrophages among Cas9 control compared with Siglec-10 knockout macrophages. Data are mean ± s.e.m. of $n = 5$ donors. **f**, Phagocytosis of wild-type MCF-7 cells by either Siglec-10 knockout or Cas9 control macrophages. Data are mean ± s.e.m. of $n = 5$ donors; paired, one-tailed Student's *t*-test, $^{**}P = 0.0035$. **g**, Flow-cytometry-based measurement of the binding of recombinant Siglec-10–Fc to MCF-7 wild-type cells treated with neuraminidase (+NA) or heat-inactivated neuraminidase (+HI-NA); plot is representative of two experimental replicates. **h**, Left, flow-cytometry-based measurement of the binding of Siglec-10–Fc to neuraminidase-treated MCF-7 wild-type cells compared with neuraminidase-treated MCF-7(ΔCD24) cells. Plot is representative of three experimental replicates. Right, normalized binding of Siglec-10–Fc to neuraminidase-treated MCF-7(ΔCD24) cells compared with neuraminidase-treated MCF-7 wild-type cells. Data are representative of three experimental replicates. **i**, Representative images from live-cell microscopy phagocytosis assays of pHrodo Red^+ MCF-7 cells treated with anti-CD24 mAb (right) or IgG control (left) at a time, *t*, of 5:05 h; images are representative of two donors and two experimental replicates.

adenocarcinoma (Panc1), pancreatic neuroendocrine tumour (APL1) and small-cell lung cancer (NCI-H82)—and no effect was observed with $CD24^-$ cells (U-87 MG) (Fig. 3b, Extended Data Fig. 5c). Upon dual treatment with CD24- and CD47-blocking antibodies, the induction of phagocytosis was increased to levels nearly 30 times that of the baseline in some cancers. Although genetic deletion of *CD47* alone did not alter the phagocytic susceptibility of MCF-7 cells, upon treatment with anti-CD24 mAb, ΔCD47 cells were more readily engulfed than were wild-type cells (Extended Data Fig. 5d). Dual treatment of pancreatic adenocarcinoma cells with anti-CD24 mAb and cetuximab enhanced phagocytosis relative to either treatment alone, demonstrating a potential synergy between anti-CD24 mAb and anti-solid-tumour mAbs (Extended Data Fig. 5e). An isotype-matched antibody against epithelial cellular adhesion molecule (EpCAM)—a surface marker that is highly expressed by MCF-7 cells—led to a modest increase in phagocytosis as compared to treatment with anti-CD24 mAb, which indicates that the vast majority of the observed increase in phagocytosis upon the addition of anti-CD24 mAb is due to loss of CD24 signalling and not due to Fc-mediated opsonization (Extended Data Fig. 6a). Both M2-like and M0 macrophages were found to respond equally to opsonization by anti-EpCAM antibodies (Extended Data Fig. 6b). Disruption of the interaction between the Fc portion of the anti-CD24 mAb and the Fc receptors—CD16 and CD32—led to a modest reduction in anti-CD24 mAb-induced phagocytosis, confirming that the Fc-mediated pro-phagocytic effect of the anti-CD24 mAb is minor (Extended Data Fig. 6c).

All Siglec-10-expressing macrophages responded to CD24 blockade (Extended Data Fig. 6d), and the magnitude of this response trended towards a correlation with Siglec-10 expression (Extended Data Fig. 6e). Genetic deletion of *SIGLEC10* led to a marked reduction in the response to CD24 blockade, which indicates that anti-CD24 mAb specifically disrupts CD24–Siglec-10 signalling (Fig. 3c). Expression of CD24 correlated with response to CD24 blockade as well as with baseline phagoytosis levels, suggesting that tissue-specific expression of CD24 is a dominant 'don't eat me' signal and highlighting the potential value of CD24 expression as a predictor of the innate anti-tumour immune response (Fig. 3d, Extended Data Fig. 6f).

Ovarian cancer cells were collected from patients with metastatic ovarian cancer and were treated with anti-CD24 mAb in order to measure phagocytosis of primary human tumours. (Fig. 3e). In these cases, CD24 blockade yielded a significantly greater effect than CD47 blockade, and dual treatment with both CD24- and CD47-blocking antibodies augmented phagocytosis at least additively (Fig. 3f). Furthermore, treatment of primary human TNBC cells with anti-CD24 mAb promoted phagocytic clearance by macrophages, whereas in these cases CD47 blockade had no effect on phagocytosis; this indicates that anti-CD24 mAb may be efficacious in cancers that show resistance to CD47 blockade (Extended Data Fig. 6g).

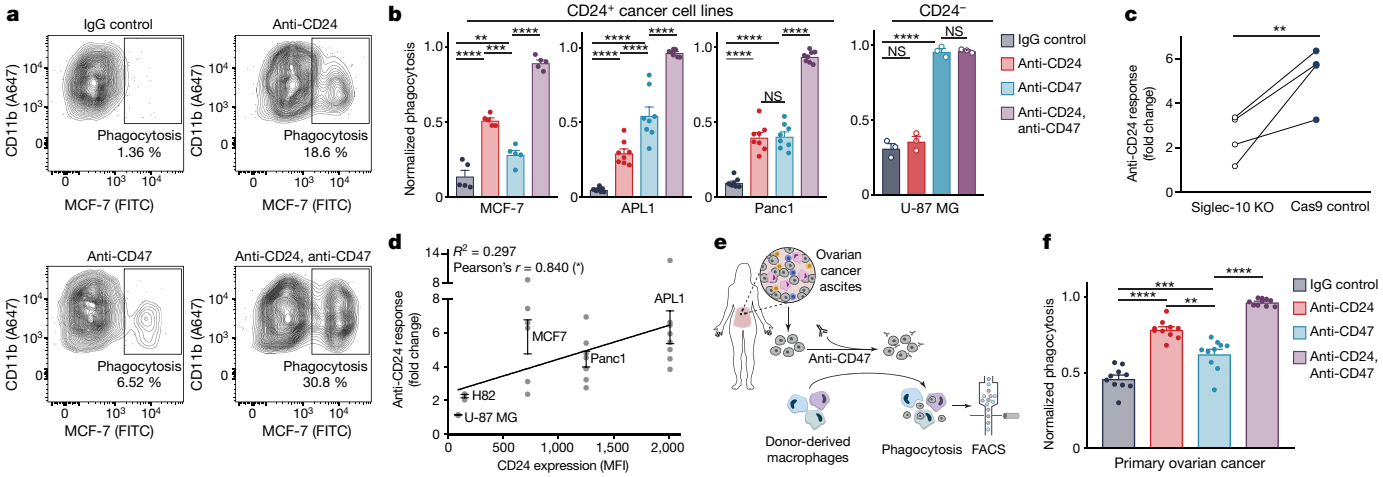

Fig. 3 | Treatment with anti-CD24 mAb promotes phagocytic clearance of human cancer cells. a, Representative flow-cytometry plots depicting the phagocytosis of MCF-7 cells treated with anti-CD24 mAb, CD47 mAb or dual treatment, compared with the IgG control. Plots are representative of five donors. FITC, fluorescein isothiocyanate. **b**, Phagocytosis of MCF-7 ($n = 5$ donors), APL1 ($n = 8$ donors) and Panc1 ($n = 8$ donors) cell lines (left) and of the U-87 GM cell line ($n = 3$ donors; solid bars) (right) in the presence of anti-CD24 mAb, anti-CD47 mAb or dual treatment, compared with IgG control (one-way ANOVA with multiple comparisons correction; MCF-7 $F_{(3,16)} = 145.6$, APL1 $F_{(3,28)} = 144.7$, Panc1 $F_{(3,28)} = 220.7$, U-87 MG $F_{(3,8)} = 200.4$; NS, not significant; $^{**}P = 0.0092$, $^{***}P = 0.0001$, $^{****}P < 0.0001$). **c**, Response to anti-CD24 mAb treatment by Siglec-10 knockout compared with Cas9 control macrophages ($n = 4$ donors, connecting lines indicate matched donor. Paired, one-tailed Student's t-test, $^{**}P = 0.0089$). **d**, Pearson correlation between CD24 expression (x axis) and mean anti-CD24 mAb response (y axis) (n values are the same as those listed in **b** and Extended Data Fig. 5c. Linear regression is shown. Data are mean ± s.e.m. $^{*}P = 0.0375$). MFI, median fluorescence intensity. **e**, Workflow to measure the phagocytosis of primary ovarian cancer. **f**, Phagocytosis of primary ovarian cancer cells treated with anti-CD24 mAb, anti-CD47 mAb or dual treatment, compared with IgG control ($n = 10$ macrophage donors, $n = 1$ primary ovarian cancer ascites donor) (one-way ANOVA with multiple comparisons correction, $F_{(2.110,\ 18.99)} = 121.5$, $^{**}P = 0.0078$, $^{***}P = 0.0006$, $^{****}P < 0.0001$). Data are mean ± s.e.m.

To investigate whether the protection against phagocytosis conferred by CD24 could be recapitulated in vivo, GFP-luciferase^{+} MCF-7 wild-type or MCF-7(ΔCD24) cells were engrafted into NOD.Cg-Prkdc^{SCID}Il2rg^{tm1Wjl}/SzJ (NSG) mice[22]. Three weeks after engraftment, we found that CD24-deficient tumours exhibited augmented levels of in vivo phagocytosis by infiltrating TAMs as compared to wild-type tumours, and TAMs that infiltrated the CD24-deficient tumours were also of a more inflammatory phenotype (Extended Data Figs. 7, 8a, b). Over weeks, we observed a robust reduction in the growth of ΔCD24 tumours as compared to wild-type tumours (Fig. 4a, b). Notably, the sublines assessed had no measurable cell-autonomous differences in proliferation in vitro (Extended Data Fig. 8c). After 35 days of growth, the polyclonal ΔCD24 tumours had become largely CD24^{+}, which is consistent with the selection against CD24^{-} cells by TAMs and the

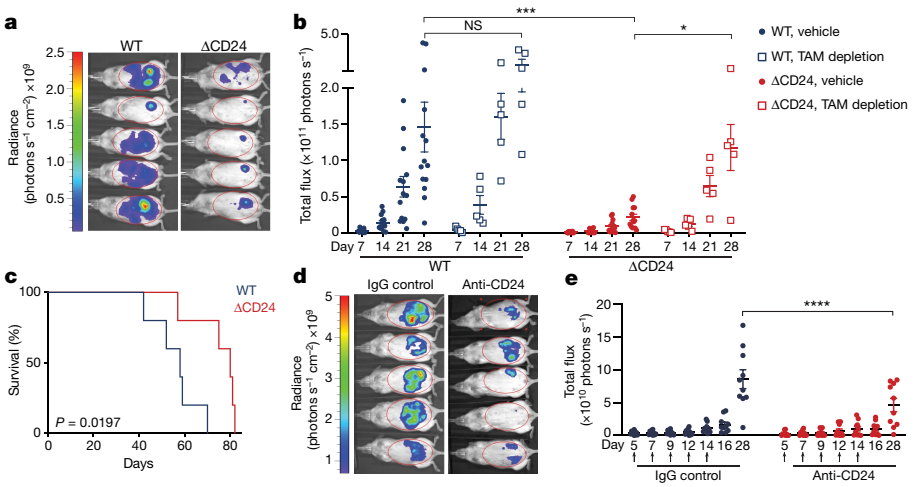

Fig. 4 | CD24 protects cancer cells from macrophage attack in vivo. **a**, Representative bioluminescence images of day-21 tumours in mice engrafted with MCF-7 wild-type and MCF-7(ΔCD24) tumours. Image representative of two independent experimental cohorts. **b**, Burden of MCF-7 wild-type compared with MCF-7(ΔCD24) tumours in mice with TAMs (vehicle) or in TAM-depleted mice (treated with anti-CSF1R) as measured by bioluminescence (WT vehicle, $n = 14$; WT TAM depletion, $n = 5$; ΔCD24 vehicle, $n = 13$; ΔCD24 TAM depletion, $n = 5$. Two-way ANOVA with multiple comparisons correction, tumour genotype $F_{(3,33)} = 11.75$, $^{*}P = 0.0296$, $^{***}P = 0.0009$). **c**, Survival analysis of vehicle-treated mice in **b**; P value computed by a log-rank (Mantel–Cox) test (WT, $n = 5$; ΔCD24, $n = 5$). **d**, Representative bioluminescence image of day-33 tumours in mice with MCF-7 tumours treated with either IgG control or anti-CD24 mAb (image representative of two experimental cohorts). Data are mean ± s.e.m. **e**, Burden of MCF-7 wild-type tumours treated with IgG control (blue) and anti-CD24 mAb (red) as measured by bioluminescence (IgG, $n = 10$; anti-CD24 mAb, $n = 10$. The days on which the treatments were administered are indicated by arrows. Data from two experimental cohorts. Two-way ANOVA with multiple-comparisons correction, tumour treatment $F_{(1,126)} = 5.679$, $^{****}P < 0.0001$).

emergence of subclones of CD24$^+$ cells that did not have biallelic *CD24* deletion (Extended Data Fig. 8d, e). TAM depletion did not significantly alter the burden of wild-type tumours, whereas the loss of TAMs largely abrogated the reduction of tumour growth that was observed in ΔCD24 tumours, indicating that increased TAM-mediated clearance of ΔCD24 cells was responsible for the diminished tumour burden (Fig. 4b, Extended Data Fig. 8f). This reduction in tumour growth—attributed to enhanced phagocytic clearance—resulted in a significant survival advantage for mice engrafted with CD24-deficient tumours (Fig. 4c).

To determine whether the mouse homologue of human CD24—gene name *Cd24a*—could similarly confer protection against phagocytic clearance of cancer cells, we generated a subline of the mouse epithelial ovarian cancer line ID8 that lacked CD24 (ID8ΔCd24a). Wild-type or ΔCd24a cells expressing GFP were injected intraperitoneally into NSG mice. After one week of growth, we observed that loss of *Cd24a* was sufficient to significantly promote in vivo phagocytosis by NSG macrophages (Extended Data Fig. 9a). To assess the effect of mouse CD24 in a syngeneic, fully immunocompetent setting, ID8 wild-type or ID8ΔCd24a cells were engrafted intraperitoneally into C57Bl/6J mice. We observed that loss of CD24 was sufficient to substantially reduce tumour growth over several weeks (Extended Data Fig. 9b, c).

To demonstrate that the enhancement of anti-tumour immunity could be modulated by therapeutic blockade of CD24, NSG mice with established MCF-7 wild-type tumours were treated with anti-CD24 monoclonal antibody for two weeks. Anti-CD24 therapy resulted in significant reduction of tumour growth compared to the IgG-treated control (Fig. 4d, e, Extended Data Fig. 9d).

Potential off-target effects of anti-CD24 mAb treatment in humans include depletion of B cells, owing to high CD24 expression by B cells. Indeed, phagocytic clearance of healthy B cells was observed upon treatment with anti-CD24 mAb (Extended Data Fig. 10a). However, we found that—unlike anti-CD47 mAbs[4]—the anti-CD24 mAb demonstrated no detectable binding to human red blood cells, even though mouse CD24a is expressed by mouse red blood cells (Extended Data Fig. 10b).

CD24 is a potent anti-phagocytic, 'don't eat me' signal that is capable of directly protecting cancer cells from attack by Siglec-10-expressing macrophages. Monoclonal antibody blockade of CD24–Siglec-10 signalling robustly enhances clearance of CD24$^+$ tumours, which indicates promise for CD24 blockade in immunotherapy. Both ovarian[23] and breast cancer have demonstrated weaker responses to anti-PD-L1/PD-1 immunotherapies than have other cancers[24–26], which suggests that an alternative strategy may be required to achieve responses across a wide range of cancers. It is notable that the 'don't eat me' signals CD47, PD-L1, B2M—and now CD24—each involve macrophage signalling based on immunoreceptor-tyrosine-based inhibition motifs. This may indicate a conserved mechanism that leads to immunoselection of the subset of macrophage-resistant cancer cells, resulting in tumours that—by nature—avoid macrophage surveillance and clearance. CD24 expression may provide immediate predictive value of the responsiveness of tumours to existing immunotherapies, in that high CD24 expression may inhibit response to therapies that are reliant on macrophage function. Expression of CD24 and CD47 was found to be inversely related among patients with diffuse large B cell lymphoma (Extended Data Fig. 10c). The percentage of patients with CD24 overexpression compares well with the response rates observed with anti-CD47 + rituximab combination therapy in this disease[4], opening up the possibility that particular tumours might respond differentially to treatment with anti-CD24 and/or anti-CD47 mAbs. Determining the collective expression of pro- and anti-phagocytic signals expressed by cancers and associated macrophages could enable better prediction of which patients may respond to treatment. This work defines CD24–Siglec-10 as an innate immune checkpoint that is essential for mediating anti-tumour immunity, and provides evidence for the therapeutic potential of CD24 blockade, with particular promise for the treatment of ovarian and breast cancers.

Online content

Any methods, additional references, Nature Research reporting summaries, source data, extended data, supplementary information, acknowledgements, peer review information; details of author contributions and competing interests; and statements of data and code availability are available at https://doi.org/10.1038/s41586-019-1456-0.

Received: 24 January 2019; Accepted: 2 July 2019;
Published online: 31 July 2019

1. Majeti, R. et al. CD47 is an adverse prognostic factor and therapeutic antibody target on human acute myeloid leukemia stem cells. *Cell* **138**, 286–299 (2009).
2. Gordon, S. R. et al. PD-1 expression by tumour-associated macrophages inhibits phagocytosis and tumour immunity. *Nature* **545**, 495–499 (2017).
3. Barkal, A. A. et al. Engagement of MHC class I by the inhibitory receptor LILRB1 suppresses macrophages and is a target of cancer immunotherapy. *Nat. Immunol.* **19**, 76–84 (2018).
4. Advani, R. et al. CD47 blockade by Hu5F9-G4 and rituximab in non-Hodgkin's lymphoma. *N. Engl. J. Med.* **379**, 1711–1721 (2018).
5. Willingham, S. B. et al. The CD47-signal regulatory protein alpha (SIRPa) interaction is a therapeutic target for human solid tumors. *Proc. Natl Acad. Sci. USA* **109**, 6662–6667 (2012).
6. Pirruccello, S. J. & LeBien, T. W. The human B cell-associated antigen CD24 is a single chain sialoglycoprotein. *J. Immunol.* **136**, 3779–3784 (1986).
7. Chen, G. Y., Brown, N. K., Zheng, P. & Liu, Y. Siglec-G/10 in self–nonself discrimination of innate and adaptive immunity. *Glycobiology* **24**, 800–806 (2014).
8. Chen, W. et al. Induction of Siglec-G by RNA viruses inhibits the innate immune response by promoting RIG-I degradation. *Cell* **152**, 467–478 (2013).
9. Chen, G. Y. et al. Amelioration of sepsis by inhibiting sialidase-mediated disruption of the CD24–SiglecG interaction. *Nat. Biotechnol.* **29**, 428–435 (2011).
10. Chen, G. Y., Tang, J., Zheng, P. & Liu, Y. CD24 and Siglec-10 selectively repress tissue damage-induced immune responses. *Science* **323**, 1722–1725 (2009).
11. Toubai, T. et al. Siglec-G–CD24 axis controls the severity of graft-versus-host disease in mice. *Blood* **123**, 3512–3523 (2014).
12. Crocker, P. R., Paulson, J. C. & Varki, A. Siglecs and their roles in the immune system. *Nat. Rev. Immunol.* **7**, 255–266 (2007).
13. Abram, C. L. & Lowell, C. A. Shp1 function in myeloid cells. *J. Leukoc. Biol.* **102**, 657–675 (2017).
14. Dietrich, J., Cella, M. & Colonna, M. Ig-like transcript 2 (ILT2)/leukocyte Ig-like receptor 1 (LIR1) inhibits TCR signaling and actin cytoskeleton reorganization. *J. Immunol.* **166**, 2514–2521 (2001).
15. Tarhriz, V. et al. Overview of CD24 as a new molecular marker in ovarian cancer. *J. Cell. Physiol.* **234**, 2134–2142 (2019).
16. Kristiansen, G. et al. CD24 expression is a new prognostic marker in breast cancer. *Clin. Cancer Res.* **9**, 4906–4913 (2003).
17. Karaayvaz, M. et al. Unravelling subclonal heterogeneity and aggressive disease states in TNBC through single-cell RNA-seq. *Nat. Commun.* **9**, 3588 (2018).
18. Mantovani, A., Sozzani, S., Locati, M., Allavena, P. & Sica, A. Macrophage polarization: tumor-associated macrophages as a paradigm for polarized M2 mononuclear phagocytes. *Trends Immunol.* **23**, 549–555 (2002).
19. Liu, J. et al. Pre-clinical development of a humanized anti-CD47 antibody with anti-cancer therapeutic potential. *PLoS ONE* **10**, e0137345 (2015).
20. Miksa, M., Komura, H., Wu, R., Shah, K. G. & Wang, P. A novel method to determine the engulfment of apoptotic cells by macrophages using pHrodo succinimidyl ester. *J. Immunol. Methods* **342**, 71–77 (2009).
21. Okazaki, M., Luo, Y., Han, T., Yoshida, M. & Seon, B. K. Three new monoclonal antibodies that define a unique antigen associated with prolymphocytic leukemia/non-Hodgkin's lymphoma and are effectively internalized after binding to the cell surface antigen. *Blood* **81**, 84–94 (1993).
22. Shultz, L. D. et al. Human lymphoid and myeloid cell development in NOD/LtSz-scid IL2R γ null mice engrafted with mobilized human hemopoietic stem cells. *J. Immunol.* **174**, 6477–6489 (2005).
23. Varga A. et al. Pembrolizumab in patients (pts) with PD-L1–positive (PD-L1$^+$) advanced ovarian cancer: updated analysis of KEYNOTE-028. *J. Clin. Oncol.* **35**, 5513 (2017).
24. Nanda, R. et al. Pebrolizumab in patients with advanced triple-negative breast cancer: Phase Ib KEYNOTE-012 study. *J. Clin. Oncol.* **34**, 2460–2467 (2016).
25. Alsaab, H. O. et al. PD-1 and PD-L1 checkpoint signaling inhibition for cancer immunotherapy: mechanism, combinations, and clinical outcome. *Front. Pharmacol.* **8**, 561 (2017).
26. Ayers M. *et al*. Molecular profiling of cohorts of tumor samples to guide clinical development of pembrolizumab as monotherapy. *Clinical Cancer Res.* https://doi.org/10.1158/1078-0432.CCR-18-1316 (2018).

METHODS

Statistics. Sample sizes were modelled after those from existing publications regarding in vitro immune killing assays and in vivo tumour growth assays, and an independent statistical method was not used to determine sample size. Statistical tests were performed in GraphPad Prism 8.

Human tumour bulk RNA-sequencing analysis. RNA-sequencing data regarding expression levels for *CD24*, *CD274* (*PD-L1*), *CD47* and *B2M* from human tumours and matched healthy tissues collected by TCGA, TARGET, and the Genotype-Tissue Expression Project (GTEX) were downloaded as $\log_2$(normalized counts +1) values from UCSC Xena[27] (https://xenabrowser.net/) with the query 'TCGA TARGET GTEX'. Tumour types were filtered for those with ≥9 individual patients for either tumour or healthy tissues. For instances in which there existed both TCGA-matched healthy tissues and GTEX healthy tissues, all healthy tissues were combined for analyses. Abbreviations for TCGA studies and number of samples analysed are listed in Supplementary Table 1. Survival analysis was performed by stratifying patients into high or low *CD24* expression using median expression values, and Kaplan–Meier plots were generated and analysed using Prism 8. Two-dimensional contour plots were generated using Plotly (Plotly Technologies)

Single-cell RNA-sequencing analysis. Raw files from previously sequenced TNBC (accession number PRJNA485423) were downloaded from the NCBI Sequence Read Archive (ref. 17). The 1,539 single-cell RNA-sequencing data was aligned to the human genome (GRCh38) using STAR (version 2.5.3a) and gene counts (gene models from ENSEMBL release 82) were determined using htseq-count (intersection-nonempty mode, secondary and supplementary alignments ignored, no quality score requirement). The expression matrix was transformed to gene counts per million (c.p.m.) sequenced reads for each cell. High-quality cells were defined as those that had at least 200,000 c.p.m. and at least 500 genes expressed. This resulted in 1,001 cells.

Marker genes used in ref. 17 were used to determine cell types. This was done using UMAP (nonlinear dimensionality reduction algorithm) on log-transformed c.p.m. values for the marker genes and labelling each of the five clusters identified on the basis of which cell markers were most expressed (see Extended Data Fig. 1d). Scatter plots were constructed using this UMAP transformation with colouring as described in the figure legends.

Cell culture. All cell lines were purchased from the American Type Culture Collection (ATCC) with the exception of the APL1 cells, which were a gift from G. Krampitz (MD Anderson), and the ID8 cells, which were obtained from the laboratory of O.D. The human NCI-H82 and APL1 cells were cultured in RPMI+GlutaMax (Life Technologies) + 10% fetal bovine serum (FBS) + 100 U ml^{-1} penicillin/streptomycin (Life Technologies). Cell lines were not independently authenticated beyond the identity provided from the ATCC. The human MCF-7, Panc1 and U-87 GM cell lines were cultured in DMEM+GlutaMax + 10% FBS + 100 U ml^{-1} penicillin/streptomycin. The murine ovarian carcinoma cell line, ID8, was cultured in DMEM + 4% FBS + 10% insulin/transferrin/selenium (Corning) + 100 U ml^{-1} penicillin/streptomycin. All cells were cultured in a humidified, 5% CO_2 incubator at 37 °C. All cell lines were tested for mycoplasma contamination.

Generation of MCF-7 and ID8 sub-lines. Parental MCF-7 and ID8 were infected with GFP–luciferase lentivirus in order to generate MCF-7-GFP-luc$^+$ and ID8-GFP-luc$^+$ cell lines, respectively. After 48 h, cells were collected and sorted by FACS in order to generate pure populations of GFP$^+$ cells. The MCF-7ΔCD24-GFP-luc$^+$ and ID8ΔCd24a-GFP-luc$^+$ sub-lines were generated by electroporating cells with recombinant CRISPR–Cas9 ribonucleoprotein (RNP), as described previously[5]. In brief, CRISPR–Cas9 guide RNA molecules targeting human *CD24* and mouse *Cd24a*, respectively, were purchased as modified, hybridized RNA molecules (Synthego) and assembled with Cas9-3NLS nuclease (IDT) via incubation at 37 °C for 45 min. Next, 2×10^6 MCF-7-GFP-luc$^+$ or ID8-GFP-luc$^+$ cells were collected, combined with corresponding complexed Cas9/RNP and electroporated using the Lonza Nucleofector IIb using Kit V (VCA-1003). After 48 h of culture, genetically modified cells were collected and purified through at least three successive rounds of FACS sorting in order to generate pure cell lines. Sequences for the single-guide RNA (sgRNA) molecules used are as follows: human *CD24* sgRNA: CGGUGCGCGGCGCGUCUAGC; *hCD47* sgRNA: AAUAGUAGCUGAGCUGAUCC; and mouse *Cd24a* sgRNA: AUAUUCUGGUUACCGGGAAA.

In vitro cell proliferation assay. Proliferation of the MCF-7 wild-type and MCF-7ΔCD24 cell lines was measured with live-cell microscopy using an Incucyte (Sartorius). Cells were each plated at around 10% confluence. Percentage confluence after cell growth was measured as per the manufacturer's instructions every 8 h for 64 h.

Neuraminidase treatment and recombinant Siglec-binding assay. MCF-7 cells were treated with either neuraminidase (from *Vibrio cholerae*, Roche) (1×10^6 cells per 100 U per ml or neuraminidase that was heat-inactivated for 15 min at 95 °C before incubation for 1 h at 37 °C in serum-free medium, after which reactions were quenched with serum before analysis. Recombinant Siglecs (10, 5 and 9) were purchased as human Fc-fusion proteins from R&D Systems. Binding of recombinant Siglecs versus human IgG1 control was assayed at a concentration of 1×10^5 cells per mg per ml at 37 °C for 1 h, in the absence of EDTA. Cells were stained with a fluorescently conjugated anti-human Fc antibody (BioLegend) to enable the measurement of recombinant Siglec binding by flow cytometry.

Macrophage generation and stimulation. Primary human donor-derived macrophages were generated as described previously[28]. In brief, leukocyte reduction system chambers from anonymous donors were obtained from the Stanford Blood Center. Peripheral monocytes were purified through successive density gradients using Ficoll (Sigma-Aldrich) and Percoll (GE Healthcare). Monocytes were then differentiated into macrophages by 7–9 days of culture in IMDM + 10% AB human serum (Life Technologies). Unless otherwise stated, macrophages used for all in vitro phagocytosis assays were stimulated with 50 ng ml^{-1} human TGFβ1 (Roche) and 50 ng ml^{-1} human IL-10 (Roche) on days 3–4 of differentiation until use on days 7–9. IL-4 stimulation was added at a concentration of 20 ng ml^{-1} on days 3–4 of differentiation until use on days 7–9.

Human macrophage knockouts. Genetic knockouts in primary human donor-derived macrophages were performed as described previously[5]. In brief, sgRNA molecules targeting the first exon of *SIGLEC10* were purchased from Synthego as modified, hybridized RNA molecules. The *SIGLEC10* sgRNA sequence used is: AGAAUCUCCCAUCCAUAGCC. Mature (day 7) donor-derived macrophages were electroporated with Cas9 ribonuclear proteins using the P3 Primary Cell Nucleofection Kit (Lonza V4XP-3024). Macrophages were collected for analysis and functional studies 72 h after electroporation. Indel frequencies were quantified using TIDE software as described previously[29].

Human samples. The Human Immune Monitoring Center Biobank, the Stanford Tissue Bank, O.D. and G. Wernig all received IRB approval from the Stanford University Administrative Panels on Human Subjects Research and complied with all ethical guidelines for human subjects research to obtain samples from patients with ovarian cancer and breast cancer, and received informed consent from all patients. Single-cell suspensions of solid tumour specimens were attained by mechanical dissociation using a straight razor, followed by an enzymatic dissociation in 10 ml of RPMI + 10 μg ml^{-1} DNaseI (Sigma-Aldrich) + 25 μg ml^{-1} Liberase (Roche) for 30–60 min at 37 °C with vigorous pipetting every 10 min to promote dissociation. After a maximum of 60 min, dissociation reactions were quenched with 4 °C RPMI + 10% FBS, filtered through a 100-μm filter and centrifuged at 400*g* for 10 min at 4 °C. Red blood cells in samples were then lysed by resuspending the tumour pellet in 5 ml ACK Lysing Buffer (Thermo Fisher Scientific) for 5 min at room temperature. Lysis reactions were quenched by the addition of 20 ml RPMI + 10% FBS, and samples were centrifuged at 400*g* for 10 min at 4 °C. Samples were either directly analysed, or resuspended in Bambanker (Wako Chemicals), aliquoted into cryovials and frozen before analysis.

FACS of primary human tumour samples. Single-cell suspensions of primary human tumour samples were obtained (described above), and frozen samples were thawed for 3–5 min at 37 °C, washed with DMEM + 10% FBS, and centrifuged at 400*g* for 5 min at 4 °C. Samples were then resuspended in FACS buffer at a concentration of 1 million cells per ml and blocked with monoclonal antibody to CD16/32 (Trustain fcX, BioLegend) for 10–15 min on ice before staining with antibody panels. Antibody panels are listed, with clones, fluorophores, usage purpose, and concentrations used in Supplementary Table 2. Samples were stained for 30 min on ice, and subsequently washed twice with FACS buffer and resuspended in buffer containing 1 μg ml^{-1} DAPI before analysis. Fluorescence compensations were performed using single-stained UltraComp eBeads (Affymetrix). Gating for immune markers and DAPI was performed using fluorescence minus one controls, while CD24$^+$ and Siglec-10$^+$ gates were drawn on the basis of appropriate isotype controls (see Extended Data Fig. 2a for gating strategy). Flow cytometry was performed either on a FACSAria II cell sorter (BD Biosciences) or on an LRSFortessa Analyzer (BD Biosciences) and all flow cytometry data reported in this work was analysed using FlowJo. Human tumour gating schemes were as follows: human TAMs: DAPI$^-$, EpCAM$^-$, CD14$^+$, CD11b$^+$; human tumour cells: DAPI$^-$, CD14$^-$, EpCAM$^+$.

Flow-cytometry-based phagocytosis assay. All in vitro phagocytosis assays reported here were performed by co-culture target cells and donor-derived macrophages at a ratio of 100,000 target cells to 50:000 macrophages for 1–2 h in a humidified, 5% CO_2 incubator at 37 °C in ultra-low-attachment 96-well U-bottom plates (Corning) in serum-free IMDM (Life Technologies). Cells with endogenous fluorescence were collected from plates using TrypLE Express (Life Technologies) before co-culture. Cells from cell lines that lack endogenous fluorescence—NCI-H82 and Panc1—were collected using TrypLE Express and fluorescently labelled with Calcein AM (Invitrogen) by suspending cells in PBS + 1:30,000 Calcein AM as per the manufacturer's instructions for 15 min at 37 °C and washed twice with 40 ml PBS before co-culture. For TNBC primary-sample phagocytosis assays, tumours were acquired fresh on the day of resection and dissociated as

described above. EpCAM$^+$ tumour cells were purified on an autoMACS pro separator (Miltenyi) by first depleting samples of myeloid cells using anti-CD14 microbeads (Miltenyi, 1:50) followed by an enrichment with anti-EpCAM microbeads (Miltenyi, 1:50). For primary ovarian cancer ascites assays, ovarian ascites samples were frozen as described above, thawed and directly labelled with Calcein-AM (Invitrogen) at a concentration of 1:30,000. For primary B cell phagocytosis assays, B cells were enriched from pooled donor peripheral blood mononuclear cell (PBMC) fractions using an autoMACS pro separator (Miltenyi) using anti-CD19 microbeads (Miltenyi, 1:50). For Fc-receptor blockade phagocytosis assays, macrophages were pre-treated with 10 μg ml^{-1} human Fc-receptor blocking solution (BioLegend) for 45 min at 4 °C, and subsequent co-culture with mAb-treated target cells was conducted in the presence of 10 μg ml^{-1} human Fc-receptor blocking solution. For all assays, macrophages were collected from plates using TrypLE Express. For phagocytosis assays involving treatment with monoclonal antibodies including anti-CD24 (Clone SN3, Novus Biologics) and anti-CD47 (Clone 5F9-G4, acquired from Forty Seven), all antibodies or appropriate isotype controls were added at a concentration of 10 μg ml^{-1}. After co-culture, phagocytosis assays were stopped by placing plates on ice, centrifuged at 400*g* for 5 min at 4 °C and stained with A647-labelled anti-CD11b (Clone M1/70, BioLegend) to identify human macrophages. Assays were analysed by flow cytometry on an LRSFortessa Analyzer (BD Biosciences) or a CytoFLEX (Beckman), both using a high-throughput auto-sampler. Phagocytosis was measured as the number of CD11b$^+$GFP$^+$ macrophages, quantified as a percentage of the total CD11b$^+$ macrophages. Each phagocytosis reaction (independent donor and experimental group) was performed in technical triplicate as a minimum, and outliers were removed using GraphPad Outlier Calculator (https://www.graphpad.com/quickcalcs/Grubbs1.cfm). To account for innate variability in raw phagocytosis levels among donor-derived macrophages, phagocytosis was normalized to the highest technical replicate per donor. All biological replicates indicate independent human macrophage donors. See Supplementary Table 2 for antibodies and isotype controls used in this study, and Extended Data Fig. 5a for example gating. Response to anti-CD24 mAb was computed by the fold change in phagocytosis between anti-CD24 mAb treatment and IgG control.

Time-lapse live-cell-microscopy-based phagocytosis assay. Non-fluorescently labelled MCF-7 cells were collected using TrypLE express and labelled with pHrodo Red succinimidyl ester (Thermo Fisher Scientific) as per the manufacturer's instructions at a concentration of 1:30,000 in PBS for 1 h at 37 °C, followed by two washes with DMEM + 10% FBS + 100 U ml^{-1} penicillin/streptomycin. Donor-derived macrophages were collected using TrypLE express and 50,000 macrophages were added to clear, 96-well flat-bottom plates and allowed to adhere for 1 h at 37 °C. After macrophage adherence, 100,000 pHrodo-Red-labelled MCF-7 cells + 10 μg ml^{-1} anti-CD24 antibody (SN3) were added in serum-free IMDM. The plate was centrifuged gently at 50*g* for 2 min in order to promote the timely settlement of MCF-7 cells into the same plane as adherent macrophages. Phagocytosis assay plates were then placed in an incubator at 37 °C and imaged at 10–20-min intervals using an Incucyte (Essen). The first image time point (reported as $t = 0$) was generally acquired within 30 min of co-culture. Images were acquired using a 20× objective at 800-ms exposures per field. Phagocytosis events were calculated as the number of pHrodo-red$^+$ events per well and values were normalized to the maximum number of events measured across technical replicates per donor. Thresholds for calling pHrodo-red$^+$ events were set on the basis of intensity measurements of pHrodo-red-labelled cells that lacked macrophages.

High-resolution phagocytosis microscopy. Fluorescently labelled MCF-7 cells (mCherry$^+$) and donor-derived macrophages were collected as described above. Suspensions consisting of 50,000 macrophages and 100,000 MCF-7 cells + 10 μg ml^{-1} antibody or isotype control in serum-free IMDM were placed into an untreated 24-well plate, in order to allow for adherence of donor-derived macrophages while preventing MCF-7 adherence. Reactions were incubated for 6 h in an incubator at 37 °C. After incubation, wells were washed vigorously five times with serum-free IMDM in order to wash away non-phagocytosed MCF-7 cells. Whole-cell phagocytosis was evaluated using a Leica DMI 6000B fluorescent microscope and an Olympus IX83. High-resolution *z*-stack images were taken on a Zeiss LSM800 confocal microscope. All images were processed in ImageJ and Adobe Illustrator.

Mice. NOD.Cg-*Prkdc*^{scid}*Il2rg*^{tm1Wjl}/SzJ (NSG) mice were obtained from in-house breeding stocks. C57Bl/6J mice were obtained from The Jackson Laboratory. All experiments were carried out in accordance with ethical care guidelines set by the Stanford University Administrative Panel on Laboratory Animal Care (APLAC). In compliance with Stanford APLAC protocol (26270), mice in long-term tumour studies were continually monitored to ensure adequate body condition scores and to ensure that tumours were less than 2.5 cm in diameter and that there was less than 50% ulceration. Female mice were used for all studies. Investigators were not blinded for animal studies.

In vivo phagocytosis analysis. For ID8 peritoneal phagocytosis analysis, 4 × 10^6, ID8-WT-GFP-luc$^+$ cells or ID8-ΔCd24a-GFP-luc$^+$ cells were engrafted into 6–8-week-old female NSG mice via intraperitoneal injection of single-cell suspensions in PBS. After 7 days, cells were collected by peritoneal lavage. For MCF-7 xenograft phagocytosis analysis, female NSG mice, 6–10 weeks of age, were engrafted with 4 × 10^6 MCF-7-WT-GFP-luc$^+$ cells or MCF-7- MCF-7-ΔCD24-GFP-luc$^+$ cells by injection of a single-cell suspension in 25% Matrigel Basement Membrane Matrix (Corning) + 75% RPMI orthotopically into the mammary fat pad. Tumours were allowed to grow for 28 days, after which tumours were resected and dissociated mechanically and enzymatically as described above. Single-cell suspensions of tumours were blocked using anti-CD16/32 (mouse TruStain FcX, BioLegend) for 15 min on ice as described above, before staining. Phagocytosis was measured as the percentage of CD11b$^+$F4/80$^+$ TAMs that were also GFP$^+$ (see Extended Data Fig. 7 for example gating). Mouse TAM gating schemes were as follows: mouse TAMs: DAPI$^-$, CD45$^+$, CD11b$^+$, F480$^+$; M1-like mouse TAMs: DAPI$^-$, CD45$^+$, CD11b$^+$, F480$^+$, CD80$^+$.

In vivo xenograft tumour-growth experiments. Female NSG mice, 6–10 weeks of age, were engrafted with 4 × 10^6 MCF-7-WT-GFP-luc$^+$ cells or MCF-7-ΔCD24-GFP-luc$^+$ cells as described above. Tumours were measured using bioluminescence imaging beginning 7 days post-engraftment and continuing every 7 days until day 28. Mice were injected intraperitoneally with firefly D-luciferin at 140 mg kg^{-1} in PBS and images were acquired 10 min after luciferin injection using an IVIS Spectrum (Perkin Elmer). Total flux was quantified using Living Image 4.0 software. For survival analyses, deaths were reported as the days on which the primary tumour burden reached 2.5 cm and/or the body condition scoring values fell below those allowed by our animal protocols.

In vivo macrophage depletion treatment study. Female NSG mice, 6–10 weeks of age, were depleted of macrophages as described previously[4] by treatment with 400 μg CSF1R antibody per mouse or PBS (vehicle) (BioXCell, Clone AFS98) three times per week for 18 days before engraftment, and throughout the duration of the experiment. Successful tissue resident macrophage depletion was confirmed by flow cytometry before tumour engraftment by peritoneal lavage and flow cytometry analysis (Extended Data Fig. 8f). Macrophage-depleted animals or vehicle treated animals were randomized before being engrafted with either MCF-7-WT-GFP-luc$^+$ or MCF-7-ΔCD24-GFP-luc$^+$ cells as described above.

Immunocompromised tumour treatment studies. Female NSG mice (6–8 weeks old) were engrafted with 4 × 10^6 MCF-7-WT-GFP-luc$^+$ cells. On day 5 after engraftment, the total flux of all tumours was measured using bioluminescence imaging and engraftment outliers were removed using GraphPad Outlier Calculator. Mice were randomized into treatment groups, receiving either anti-CD24 monoclonal antibody (clone SN3, Creative Diagnostics) or mouse IgG1 isotype control (clone MOPC-21, BioXcell). On day 5 after engraftment, mice received an initial dose of 200 μg and were subsequently treated every other day at a dose of 400 μg for two weeks. Bioluminescence imaging was performed throughout the study and after treatment withdrawal in order to assess tumour growth.

In vivo immunocompetent growth experiments. Female C57Bl/6 mice, 6–8 weeks of age were injected intraperitoneally with 1 × 10^6 ID8-WT-tdTomato-luc$^+$ or ID8-ΔCd24a-tdTomato-luc$^+$ cells in PBS. Tumour growth was measured by weekly bioluminescence imaging, beginning two weeks after engraftment.

Reporting summary. Further information on research design is available in the Nature Research Reporting Summary linked to this paper.

Data availability

All primary data for all figures and supplementary figures are available from the corresponding authors upon request.

27. Goldman, M., Craft, B., Brooks, A. N., Zhu, J. & Haussler, D. The UCSC Xena Platform for cancer genomics data visualization and interpretation. Preprint at https://doi.org/10.1101/326470v3 (2018).
28. Martinez, F. O. Analysis of gene expression and gene silencing in human macrophages. *Curr. Protoc. Immunol.* **96**, 14.28.1–14.28.23 (2012)
29. Brinkman, E. K., Chen, T., Amendola, M. & van Steensel, B. Easy quantitative assessment of genome editing by sequence trace decomposition. *Nucleic Acids Res.* **42**, e168 (2014).

Acknowledgements We thank the members of the Weissman laboratory, the Stanford Stem Cell Institute, R. L. Maute and K. S. Kao for advice and discussions; A. McCarty, T. Naik and L. Quinn for technical and logistical support; I. Wapnir for providing samples from patients with breast cancer; G. Wernig for providing human ascites samples; and G. Krampitz for the APL1 cell line. The research reported in this publication was supported by the Virginia D. K. Ludwig Fund for Cancer Research (NIHR01CA086017 and NIHGR01GM100315) and the NIH/NCI Outstanding Investigator Award (R35CA220434 to I.L.W.); the Stanford Medical Scientist Training Program (T32GM007365 to A.A.B); the National Cancer Institute (F30CA232472 to A.A.B); and the Program in Translational and Experimental Hematology T32

from the National Heart, Lung, and Blood Institute (1T32HL120824 to B.W.Z.). The contents of this manuscript are solely the responsibility of the authors.

Author contributions A.A.B. wrote the manuscript. A.A.B. and I.L.W. conceived and designed all experiments. A.A.B., R.E.B. and M.M. performed all flow cytometry analyses, generated human macrophages, and performed in vitro phagocytosis assays. A.A.B., R.E.B. and M.M. performed in vivo experiments and S.A.B. assisted with in vivo phagocytosis measurements. B.W.Z. assisted with the design of neuraminidase experiments. M.K. performed single-cell RNA-sequencing analysis. J.H. assisted with live-cell microscopy. L.J.B. assisted with statistical analysis and manuscript preparation. O.D. and V.K. provided primary human ovarian cancer samples. I.L.W. supervised the research and edited the manuscript.

Competing interests A.A.B. and I.L.W. are co-inventors on a patent application (62/684,407) related to this work. I.L.W. is a founder, director, stockholder and consultant of Forty Seven, a cancer immunotherapy company.

Additional information

Supplementary information is available for this paper at https://doi.org/10.1038/s41586-019-1456-0.

Correspondence and requests for materials should be addressed to I.L.W.

Peer review information *Nature* thanks Gregory Beatty, Heinz Läubli and the other, anonymous, reviewer(s) for their contribution to the peer review of this work.

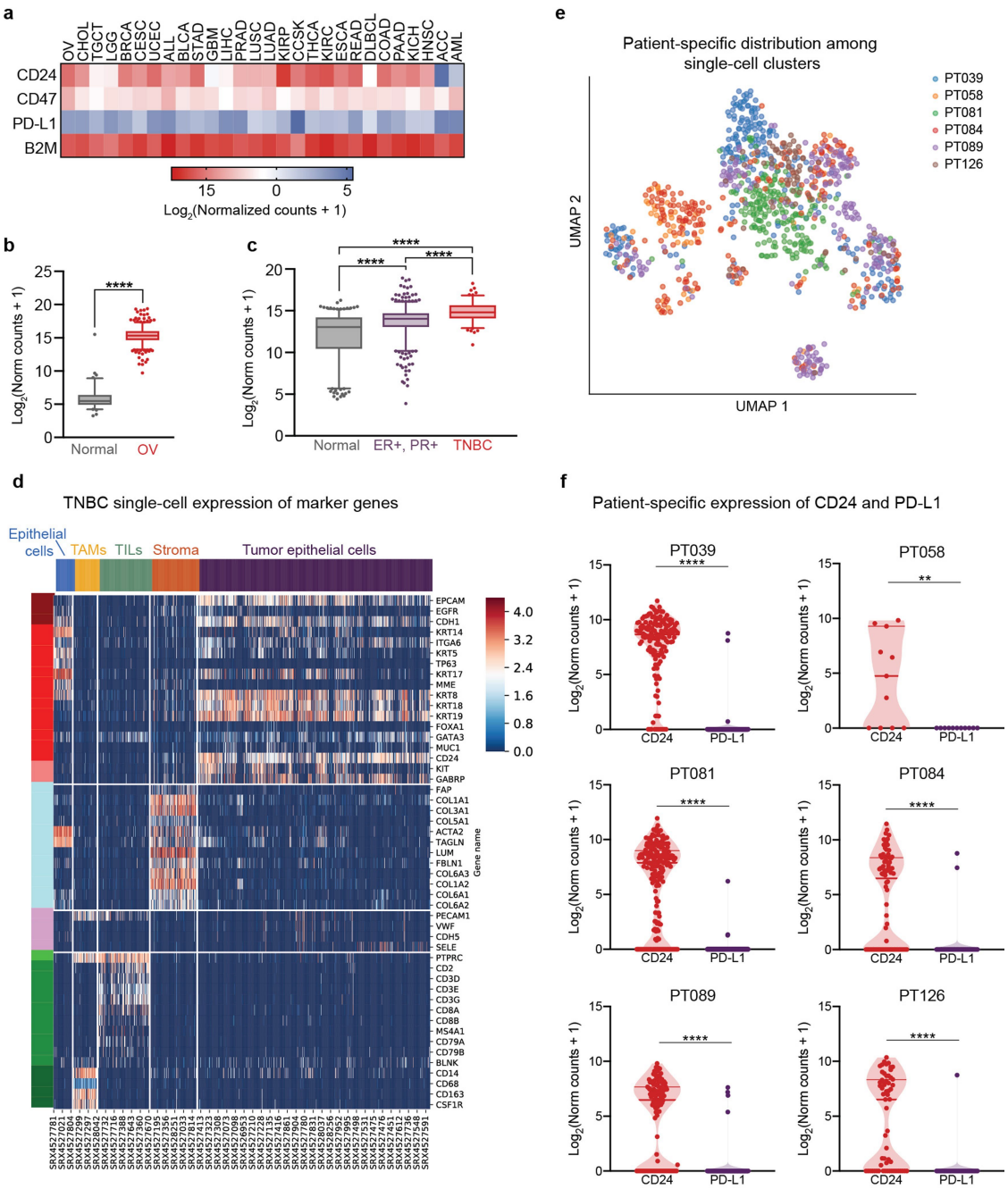

Extended Data Fig. 1 | Expression of innate immune checkpoints in human cancer. a, Heat map of expression ($\log_2$(normalized counts + 1)) of *CD24* from bulk TCGA and TARGET studies, as compared to known innate immune checkpoint molecules *CD47*, *PD-L1* and *B2M* (tumour study abbreviations and *n* values are defined in Supplementary Table 1). **b**, Expression levels of *CD24* in ovarian cancer (OV, red box plot, $n = 419$) in comparison with ovarian tissue from healthy individuals (grey box plot, $n = 89$), boxes show the median and whiskers indicate the 95th and 5th percentiles, $^{****}P < 0.0001$, unpaired, two-tailed Student's *t*-test. **c**, Expression levels of *CD24* in TNBC (red box plot, $n = 124$) in comparison with ER^+PR^+ breast cancer (purple box plot, $n = 508$) and healthy breast cells (grey box plot, $n = 293$). Each symbol represents an individual patient sample, boxes show the median and whiskers indicate the 95th and 5th percentiles, $^{****}P < 0.0001$, one-way ANOVA with multiple comparisons correction, $F_{(2,922)} = 95.80$. **d**, Heat map of marker gene expression (*y* axis) across TNBC single cells (*x* axis) and cell clusters identified (top). **e**, UMAP dimension 1 and 2 plots displaying all TNBC cells analysed from six patients ($n = 1{,}001$ single cells); cell clusters are coloured by cell patient (for key, see right). **f**, *CD24* compared with *PD-L1* expression in the 'Tumour epithelial cell' cluster for individual TNBC patients. Number of single cells analysed: PT039, $n = 151$ cells; PT058, $n = 11$ cells; PT081, $n = 196$ cells; PT084, $n = 84$ cells; PT089, $n = 117$ cells; PT126, $n = 60$ cells. $^{**}P < 0.01$, $^{****}P < 0.0001$. Data are violin plots showing median expression ($\log_2$(normalized counts +1)) and quartiles (paired, two-tailed *t*-test).

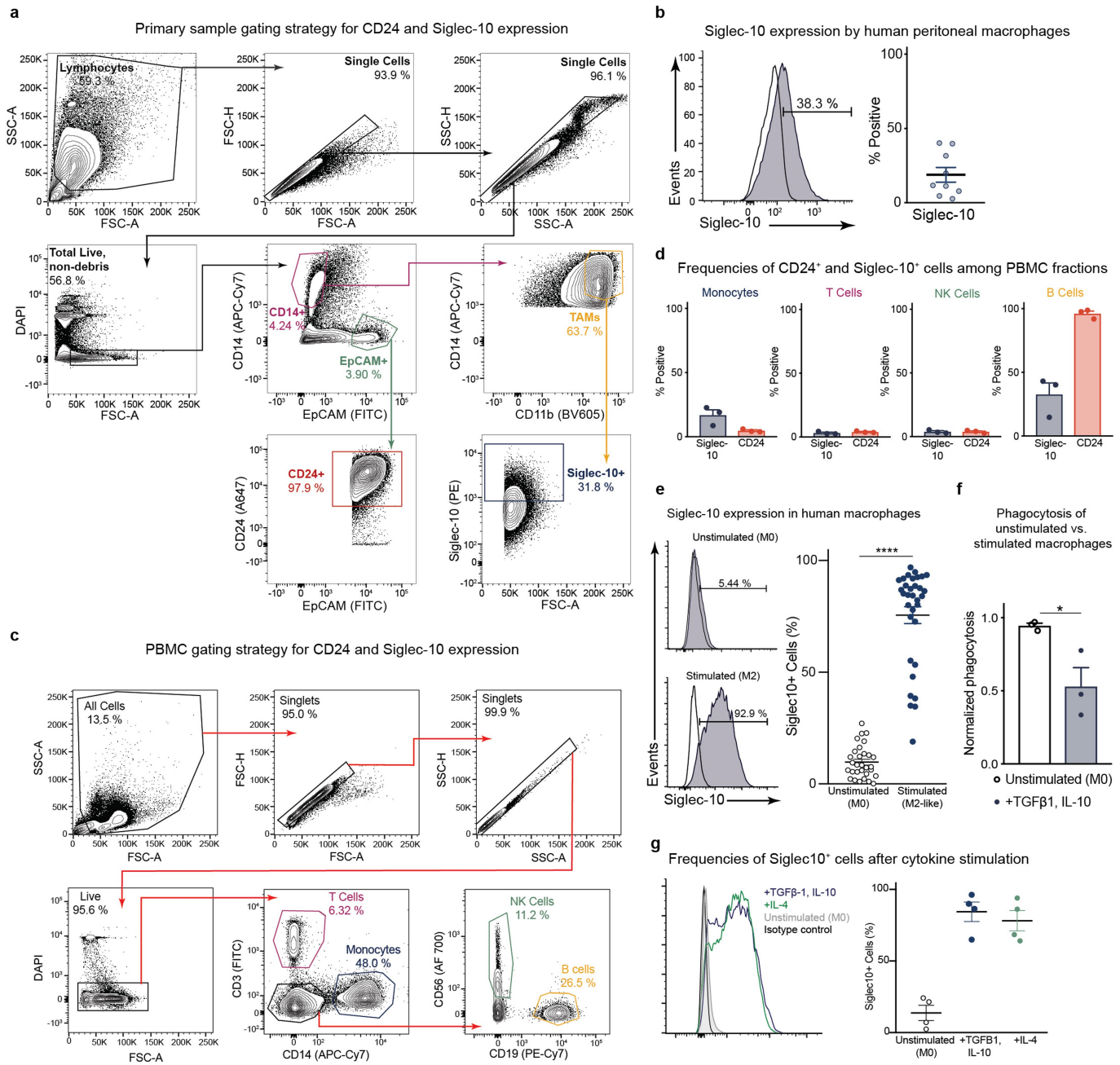

Extended Data Fig. 2 | Flow-cytometry analysis of CD24 and Siglec-10 expression in human tumours and primary immune cells. **a**, Gating strategy for $CD24^+$ cancer cells and Siglec-10^+ TAMs in primary human tumours; after debris and doublet removal, cancer cells were assessed as $DAPI^-CD14^-EpCAM^+$ and TAMs were assessed as $DAPI^-EpCAM^-CD14^+CD11b^+$. Plots are representative of six experimental replicates. **b**, Left, representative flow-cytometry histogram measuring the expression of Siglec-10 (blue shaded curves) versus isotype control (black lines) by non-cancerous peritoneal macrophages; numbers above bracketed line indicate the percentage of macrophages positive for expression of Siglec-10. Right, frequency of peritoneal macrophages positive for Siglec-10 among all peritoneal macrophages as defined by isotype controls ($n = 9$ donors). **c**, Gating strategy for $CD24^+$ cells and Siglec-10^+ cells among PBMC cell types; after debris and doublet removal, monocytes were assessed as $DAPI^-CD3^-CD14^+$; T cells were assessed as $DAPI^-CD14^-CD3^+$; natural killer (NK) cells were assessed as $DAPI^-CD14^-CD3^-CD56^+$; B cells were assessed as $DAPI^-CD56^-CD14^-CD3^-CD19^+$. Plots are representative of two experimental replicates. **d**, Frequency of PBMC cell types positive for Siglec-10 (blue shaded bars) or CD24 (red shaded bars) out of total cell type ($n = 3$ donors). **e**, Left, flow-cytometry-based measurement of the surface expression of Siglec-10 on primary human donor-derived macrophages either unstimulated (top) or after stimulation with M2-polarizing cytokines TGFβ1 and IL-10 (bottom), numbers above bracketed line indicate the per cent of $CD11b^+$ macrophages positive for expression of Siglec-10. Right, frequency of primary human donor-derived macrophages positive for Siglec-10 either without stimulation (unstimulated, M0) or following stimulation with TGFβ1 and IL-10 (stimulated, M2-like) ($n = 30$ unstimulated donors, 33 stimulated donors; unpaired, two-tailed Student's t-test, $^{****}P < 0.0001$, data are mean ± s.e.m.). **f**, Flow-cytometry-based measurement of phagocytosis of MCF-7 cells by unstimulated donor-derived macrophages (white data points) versus TGFβ1 and IL-10-stimulated donor-derived macrophages ($n = 3$ donors, unpaired, one-tailed t-test, $^*P = 0.0168$). **g**, Left, flow-cytometry-based measurement of the surface expression of Siglec-10 on matched, primary donor-derived macrophages either unstimulated (grey shaded curve), or after stimulation with TGFβ1 and IL-10 (blue line), or IL-4 (green line). Right, frequency of matched, human donor-derived macrophages positive for Siglec-10 either without stimulation (unstimulated, M0), or after stimulation with TGFβ1 and IL-10 (blue dots), or stimulated with IL-4 ($n = 4$ donors). Data are mean ± s.e.m.

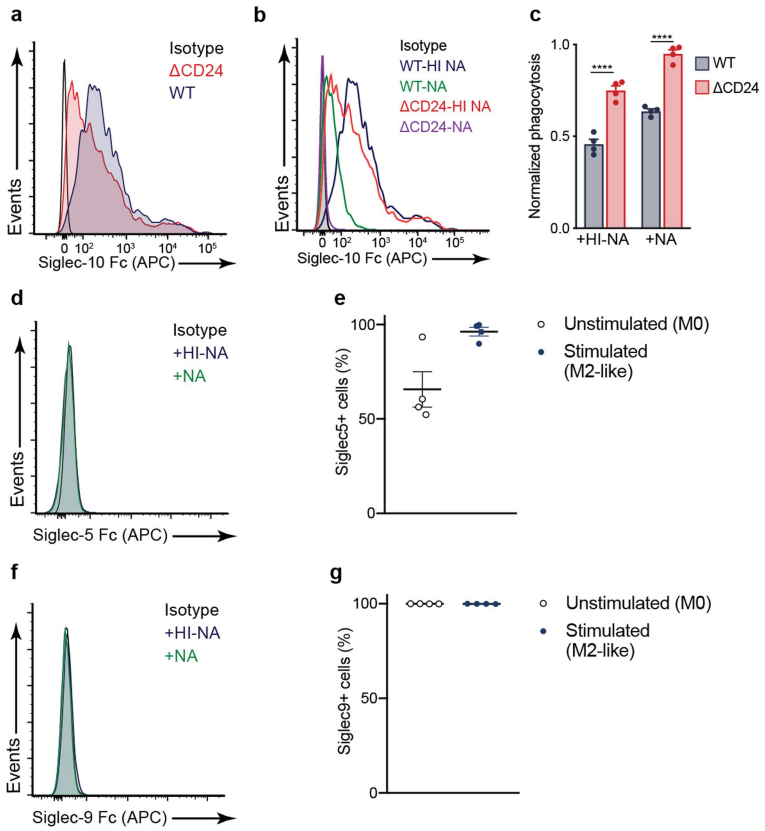

Extended Data Fig. 3 | Siglec-10 binds to CD24 expressed on MCF-7 cells. a, Flow cytometry histogram measuring the binding of Siglec-10 to wild-type MCF-7 cells (blue shaded curve) versus MCF-7(ΔCD24) cells (red shaded curve). Data are representative of two experimental replicates. **b**, Merged flow cytometry histogram measuring the binding of Siglec-10–Fc to wild-type MCF-7 cells treated with heat-inactivated neuraminidase (WT-HI NA, blue line), wild-type MCF-7 cells treated with neuraminidase (WT-NA, green line), MCF-7(ΔCD24) cells treated with heat-inactivated neuraminidase (red line, ΔCD24-HI NA), and MCF-7(ΔCD24) cells treated with neuraminidase (purple line, ΔCD24-NA) as compared to isotype control (black line). Data are representative of two experimental replicates. **c**, Flow-cytometry-based measurement of phagocytosis of $CD24^+$ parental MCF-7 cells (WT) and $CD24^-$ (ΔCD24) MCF-7 cells by co-cultured human macrophages in the presence of neuraminidase (+NA) or heat-inactivated neuraminidase (+HI-NA) ($n = 4$ donors; two-way ANOVA with multiple comparison's correction, cell line $F_{(1,12)} = 180.5$, treatment $F_{(1,12)} = 71.12$, $^{****}P < 0.0001$, data are mean ± s.e.m.). **d**, **f**, Representative flow cytometry histogram measuring the binding of Siglec-5 (**d**) or Siglec-9 (**f**) to wild-type MCF-7 cells treated with either vehicle (blue shaded curve) or neuraminidase (green shaded curve). Data are representative of two experimental replicates. **e**, **g**, Frequency of macrophages positive for Siglec-5 (**e**) or Siglec-9 (**g**) among unstimulated M0 macrophages or stimulated M2-like macrophages ($n = 4$ donors). Data are mean ± s.e.m.

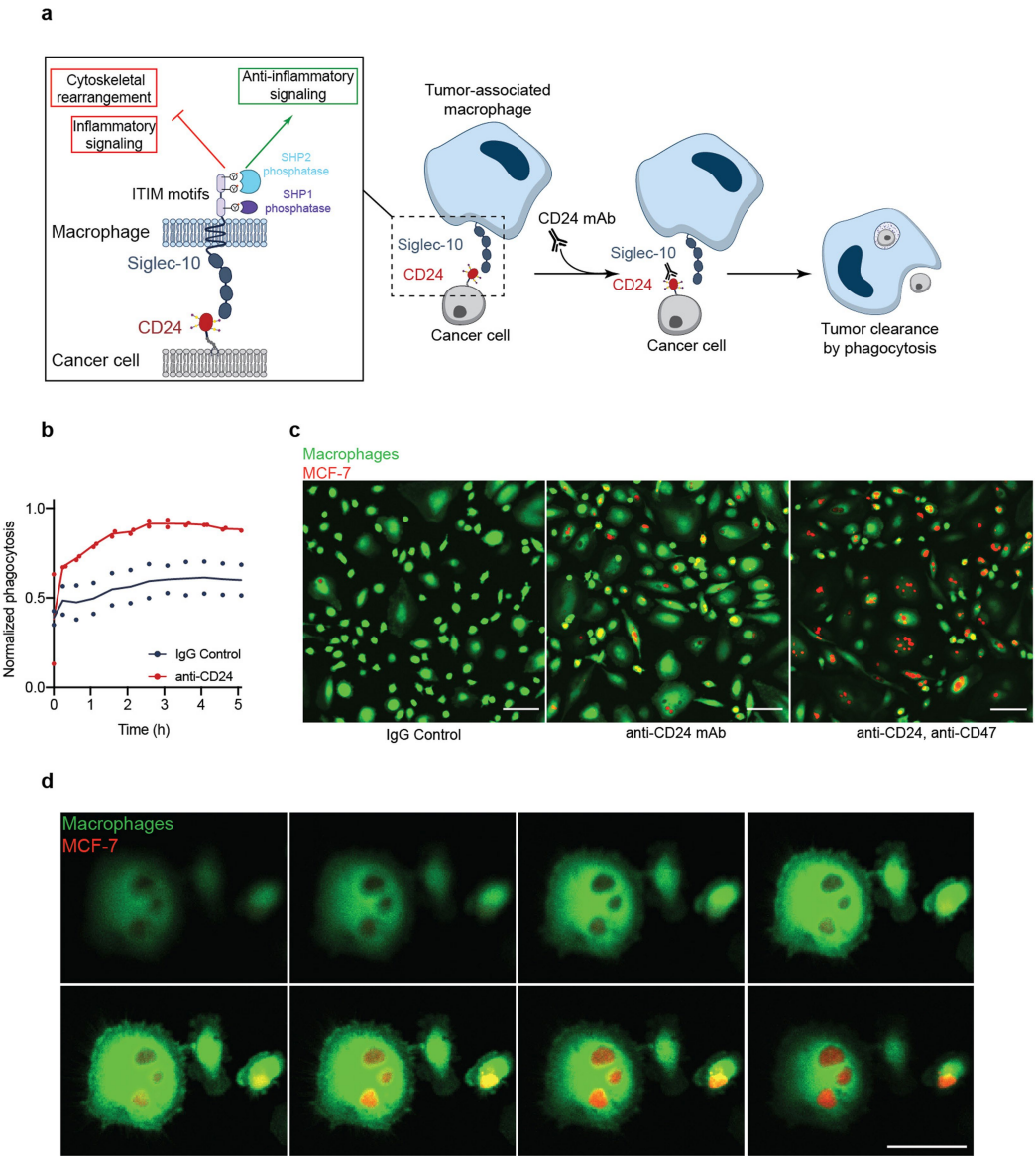

Extended Data Fig. 4 | Anti-CD24 monoclonal antibodies promote phagocytic clearance of cancer cells over time. a, Schematic of the inhibition of phagocytosis by CD24–Siglec-10. The inhibitory receptor Siglec-10 engages its ligand CD24 on cancer cells, leading to phosphorylation of the two immunoreceptor tyrosine-based inhibition motifs in the cytoplasmic domain of Siglec-10 and subsequent anti-inflammatory, anti-phagocytic signalling cascades mediated by SHP-1 and SHP-2 phosphatases; upon the addition of a CD24 blocking antibody, macrophages are disinhibited and are thus capable of phagocytosis-mediated tumour clearance. **b**, Quantification of phagocytosis events of MCF-7 cells treated with anti-CD24 mAb (red curve) versus IgG control (blue curve) as measured by live-cell microscopy over time, normalized to maximum measured phagocytosis events per donor (n = two donors; P value computed by two-way ANOVA of biological replicates, $F_{(1,24)} = 65.02$). Line is the mean of two biological replicates with individual replicates shown. **c**, Representative fluorescence microscopy images of in vitro phagocytosis of MCF-7 cells (mCherry$^+$, red) by macrophages (Calcein, AM; green) in the presence of IgG control (left), anti-CD24 mAb (middle), or anti-CD24 mAb and anti-CD47 mAb (right), after 6 h of co-culture. Experiment was repeated with three donors. Scale bar, 100 μm. **d**, Representative Z-stack images collected from high-resolution confocal fluorescence microscopy of macrophage phagocytosis demonstrating engulfment of whole MCF-7 cells (mCherry$^+$, red) by macrophages (Calcein, AM; green). Experiment was repeated with three donors. Scale bar, 50 μm.

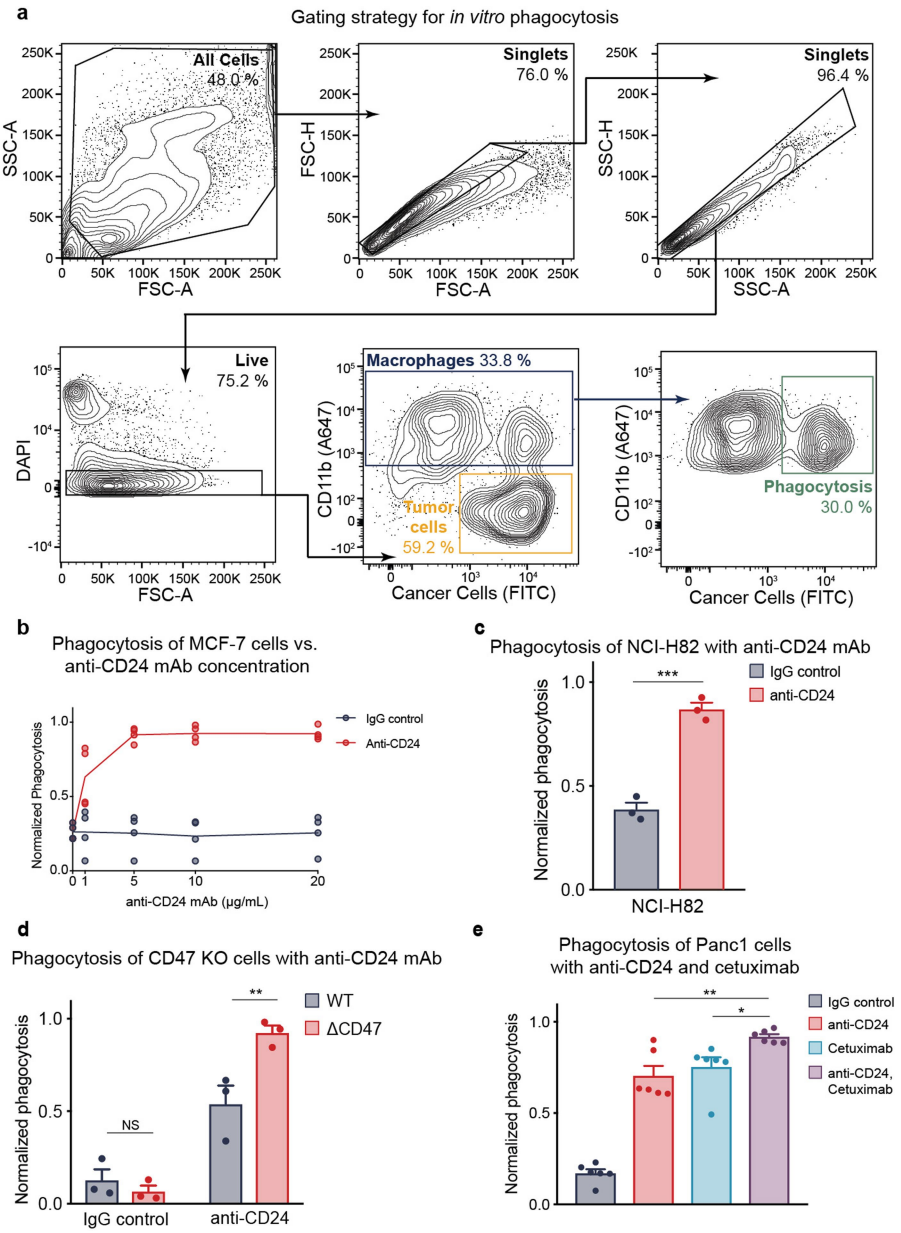

Extended Data Fig. 5 | CD24 antibody blockade of CD24–Siglec-10 signalling promotes dose-responsive enhancement of phagocytosis. **a**, Gating strategy for in vitro phagocytosis assay. Following debris and doublet removal, phagocytosis was assessed as the frequency of $DAPI^{-}CD11b^{+}FITC^{+}$ events out of all $DAPI^{-}CD11b^{+}$ events. Numbers indicate frequency of events out of previous gate. Plots are representative of at least 10 experimental replicates. **b**, Dose–response relationship of anti-CD24 mAb on phagocytosis of MCF-7 cells, concentrations listed on the *x* axis as compared to IgG control ($n = 3$ donors). Connecting line is mean. **c**, Flow-cytometry-based measurement of phagocytosis of NCI-H82 cells by donor-derived macrophages ($n = 3$ donors) in the presence of anti-CD24 mAb as compared to IgG control; each symbol represents an individual donor (paired, two-tailed Student's *t*-test, $***P = 0.0001$). Data are mean ± s.e.m. **d**, Flow-cytometry-based measurement of phagocytosis of $CD24^{+}$ parental MCF-7 cells (WT) and $CD47^{-}$ (ΔCD47) MCF-7 cells by co-cultured human macrophages, in the presence or absence of anti-CD24 mAb (horizontal axis), ($n = 4$ donors; two-way ANOVA with multiple comparisons correction, cell line $F_{(1,8)} = 6.490$; treatment $F_{(1,8)} = 98.73$, $**P = 0.0054$). Data are mean ± s.e.m. **e**, Flow-cytometry-based measurement of phagocytosis of Panc1 pancreatic adenocarcinoma cells in the presence of anti-CD24 mAb, cetuximab (anti-EGFR), or both anti-CD24 mAb and cetuximab, as compared to IgG control ($n = 6$ donors) (one-way ANOVA with multiple comparisons correction, $F_{(3,20)} = 66.10$, $*P = 0.0373$, $**P = 0.0057$, data are mean ± s.e.m.).

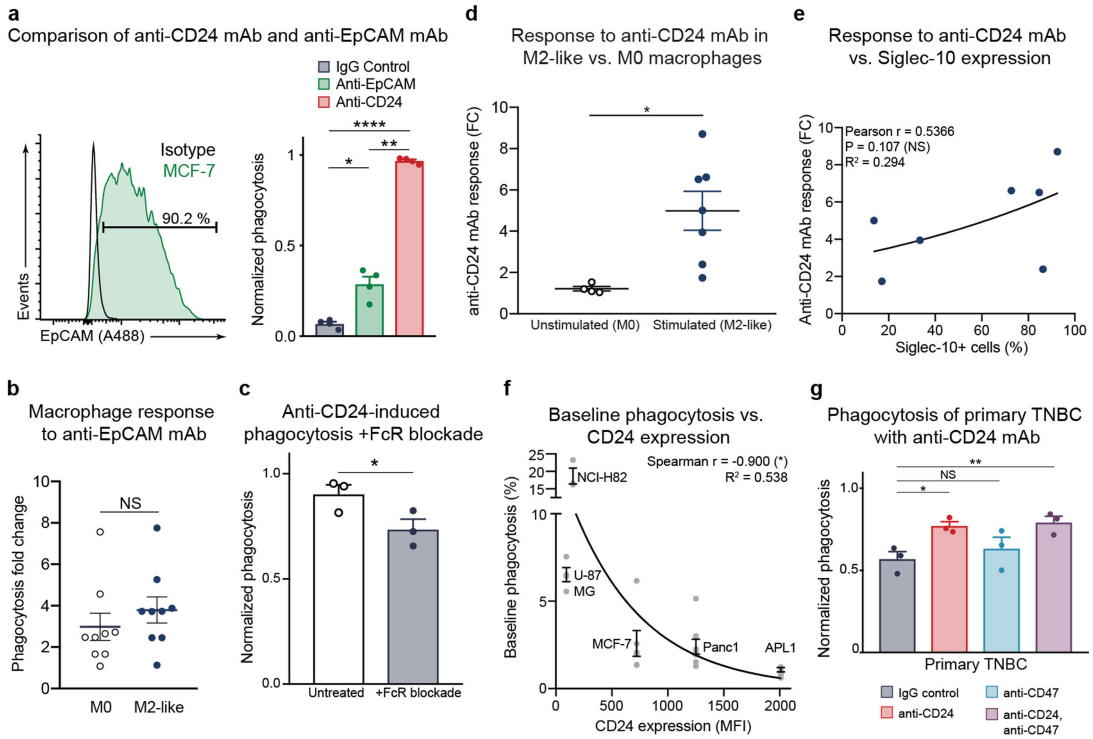

Extended Data Fig. 6 | The opsonization effect of anti-CD24 mAb is minor and CD24 blockade promotes phagocytosis of primary TNBC. a, Left, representative flow cytometry histogram measuring the expression of EpCAM (green shaded curve) by parental MCF-7 cells; number above bracketed line indicates the percentage of MCF-7 cells positive for expression of EpCAM. Right, flow cytometry–based measurement of phagocytosis of parental MCF-7 cells by co-cultured human macrophages, in the presence of either IgG control, anti-EpCAM mAb or anti-CD24 mAb ($n = 4$ donors; repeated measures ANOVA with multiple comparisons correction, $F_{(2,9)} = 340.9$, $^{*}P = 0.0287$, $^{**}P = 0.0015$, $^{****}P < 0.0001$). Data are mean ± s.e.m. **b**, Fold change in phagocytosis by M0 (unstimulated) or M2-like (TGFβ1, IL-10-stimulated) macrophages upon the addition of anti-EpCAM mAb as compared to IgG control ($n = 9$ donors, paired, two-tailed t-test). Data are mean ± s.e.m. **c**, Flow-cytometry-based measurement of anti-CD24 mAb-induced phagocytosis of MCF-7 cells by untreated macrophages (white bar) versus macrophages treated with anti-CD16/32 mAb (+FcR blockade, blue bar) ($n = 3$ macrophage donors. Paired, two-tailed t-test. Each point represents an individual donor. $^{*}P = 0.0358$). Data are mean ± s.e.m. **d**, Response to anti-CD24 mAb by M2-like macrophages compared with M0 macrophages; each symbol represents an individual donor ($n = 4$, M0 donors; $n = 6$, M2-like donors; unpaired, two-tailed Student's t-test, $^{*}P = 0.0160$). **e**, Pearson correlation between stimulated (M2-like) donor-derived macrophage Siglec-10 expression and response to anti-CD24 mAb as computed by the phagocytosis fold change between anti-CD24 mAb treatment and IgG control ($n = 7$ donors); exponential growth curve is shown. **f**, Spearman correlation between cancer cell CD24 expression and baseline, un-normalized phagocytosis levels (IgG control) averaged across all donors per cell line. Exponential growth equation is shown (n values are the same as in Fig. 3b and Extended Data Fig. 5c, $^{*}P = 0.0417$). Data are mean ± s.e.m. **g**, Flow-cytometry-based measurement of phagocytosis of a sample of primary TNBC cells from a patient, in the presence of anti-CD24 mAb, anti-CD47 mAb, or both anti-CD24 mAb and anti-CD47 mAb, as compared to IgG control ($n = 3$ macrophage donors challenged with $n = 1$ primary TNBC donor; repeated-measures one-way ANOVA with multiple comparisons correction, $F_{(1.217,2.434)} = 26.17$). Each point represents an individual donor. $^{*}P = 0.0434$, $^{**}P = 0.0028$. Data are mean ± s.e.m.

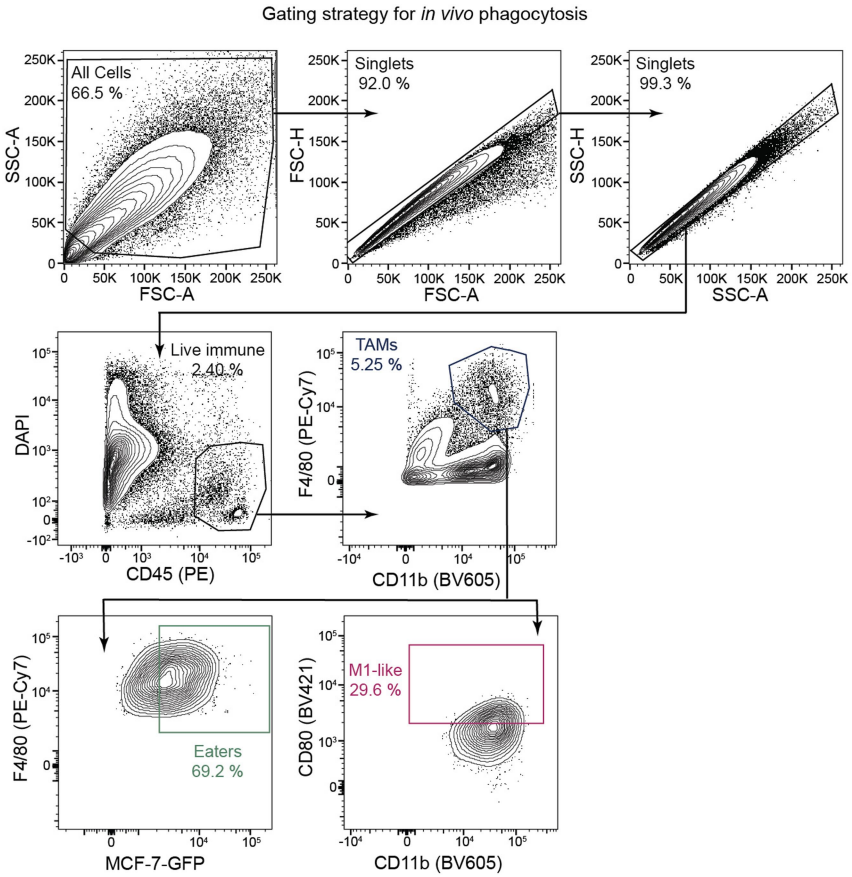

Extended Data Fig. 7 | Gating strategy for in vivo phagocytosis. Gating strategy for in vivo TAM phagocytosis of MCF-7 cells; after debris and doublet removal, TAM phagocytosis is assessed as the frequency of $DAPI^{-}CD11b^{+}F4/80^{+}GFP^{+}$ events out of total $DAPI^{-}CD11b^{+}F4/80^{+}$ events; M1-like TAMs assessed as $DAPI^{-}CD11b^{+}F4/80^{+}CD80^{+}$, numbers indicate frequency of events out of the previous gate. Plots are representative of three experimental replicates.

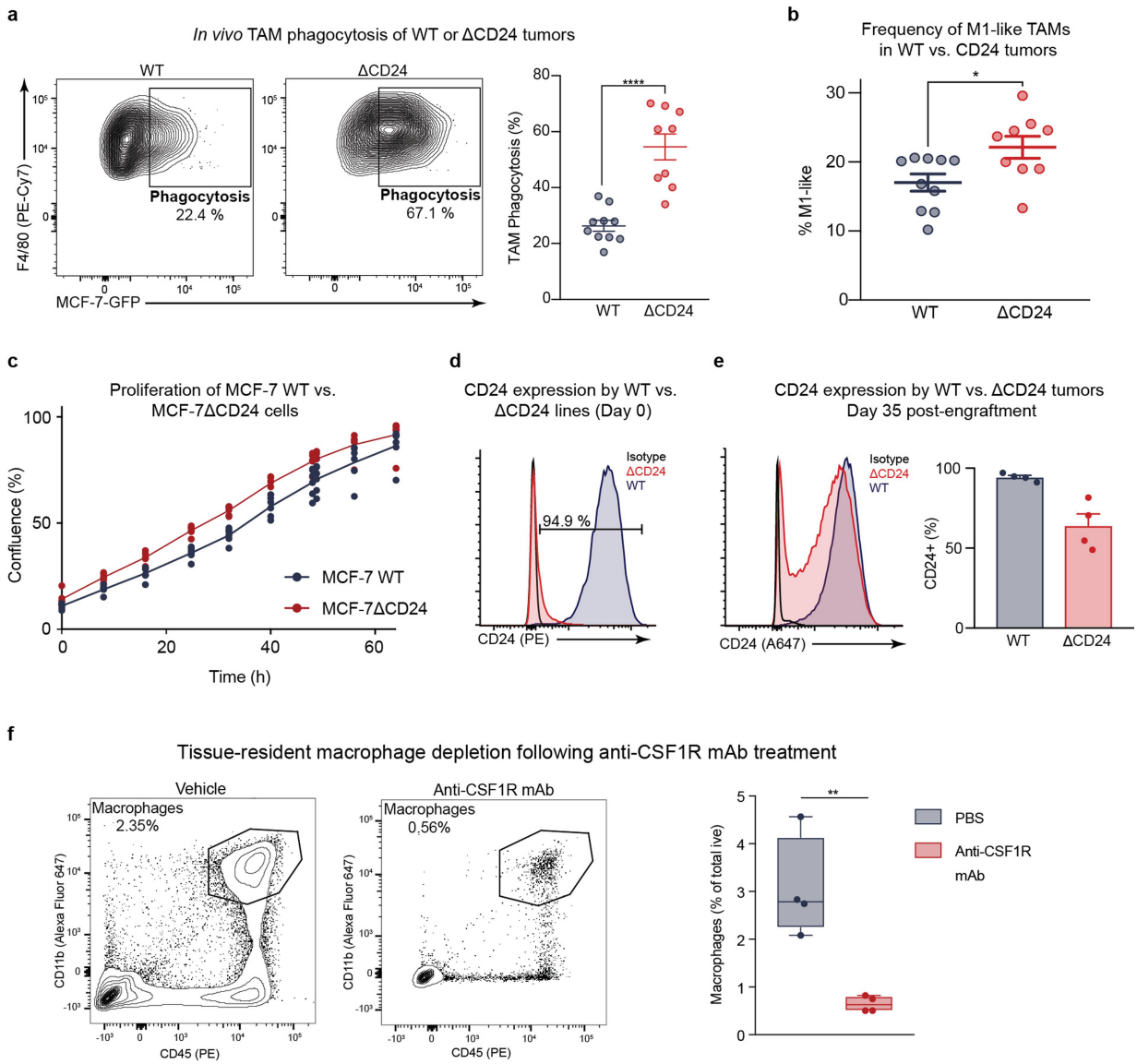

Extended Data Fig. 8 | Characterization of MCF-7 wild-type and MCF-7(ΔCD24) cells in vitro and in vivo. a, Representative flow cytometry plots demonstrating TAM phagocytosis in GFP-luciferase^{+}CD24^{+} (WT) MCF-7 tumours (left) versus CD24^{-} (ΔCD24) MCF-7 tumours (middle), numbers indicate frequency of phagocytosis events out of all TAMs. Right, frequency of phagocytosis events out of all TAMs in wild-type tumours versus ΔCD24 tumours 28 days after engraftment (WT, $n = 10$; ΔCD24, $n = 9$; unpaired, two-tailed Student's t-test, $^{****}P < 0.0001$). **b**, Frequency of TAMs positive for CD80 (M1-like) as per gating in **a**, among all TAMs macrophages as defined by fluorescence minus one controls (WT, $n = 10$; ΔCD24, $n = 9$; unpaired, two-tailed Student's t-test, $^{*}P < 0.0203$). Data are mean ± s.e.m. **c**, In vitro proliferation rates of MCF-7 wild-type and MCF-7(ΔCD24) as assessed by a plot of confluence percentage over time ($n = 6$ technical replicates, one experimental replicate). Individual technical replicates are shown, the connecting line indicates the mean. **d**, Flow-cytometry-based measurement of the surface expression of CD24 on MCF-7 cells (blue shaded curve) versus CD24 knockout cells (ΔCD24) (red shaded curve) before tumour engraftment as compared to isotype control (black line), numbers above the bracketed line indicate the percentage of MCF-7 wild-type cells positive for expression of CD24. The plot is representative of ten experimental replicates. **e**, Left, representative flow-cytometry histogram of the surface expression of CD24 on day-35 wild-type MCF-7 tumours (blue shaded curve) versus day-35 CD24 knockout tumours (ΔCD24) (red shaded curve) as compared to isotype control (black line). Right, flow-cytometry-based measurement of the frequency of CD24^{+} cells among all cancer cells in day-35 wild-type tumours versus day 35 ΔCD24 tumours (WT, $n = 4$; ΔCD24, $n = 4$). Data are mean ± s.e.m. **f**, Representative flow cytometry plots of tissue-resident macrophages out of total live cells in vehicle-treated mice (left) compared with anti-CSF1R-treated mice (middle); numbers indicate frequency of CD11b^{+}F4/80^{+} macrophage events out of total live events. Right, frequency of TAMs (CD11b^{+}F4/80^{+}) out of total live cells in vehicle-treated mice ($n = 5$, blue shaded box plot) versus anti-CSF1R-treated mice ($n = 4$, red shaded box plot) as measured by flow cytometry. $^{**}P < 0.01$. Box plots depict mean and range.

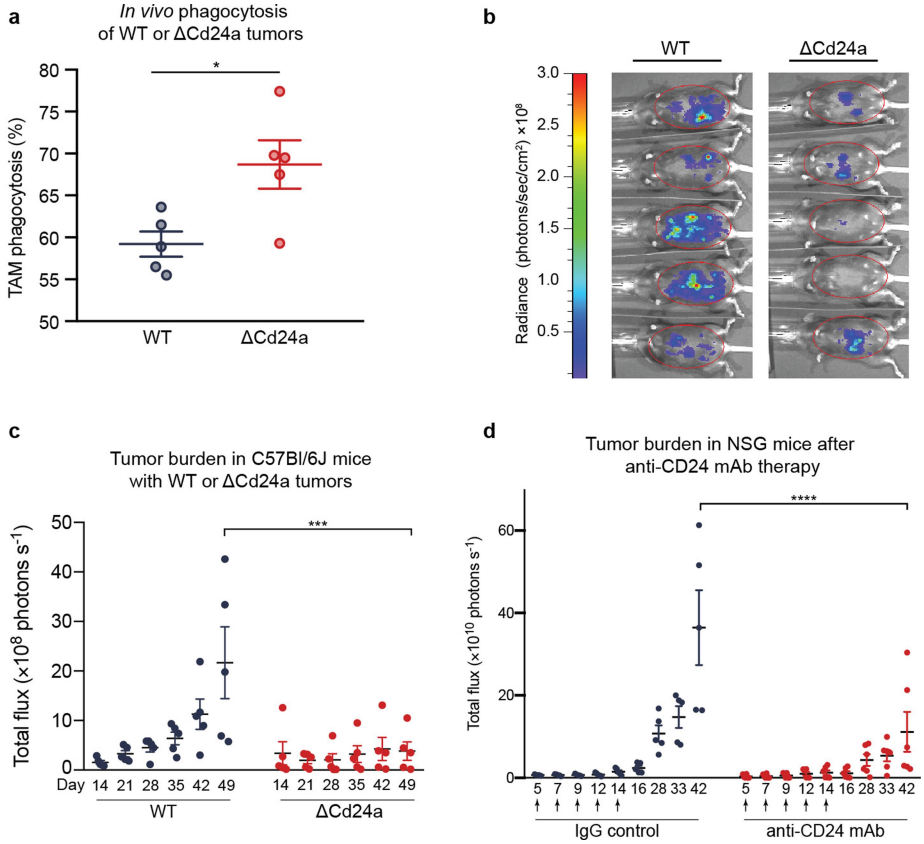

Extended Data Fig. 9 | Validation of CD24 inhibition in in vivo models of ovarian and breast cancer. a, In vivo phagocytosis of wild-type or ΔCd24a cancer cells by mouse TAMs. Flow cytometry–based measurement of in vivo phagocytosis of $CD24^{+}GFP^{+}$ ID8 cells (WT) versus $CD24^{-}GFP^{+}$ ID8 cells (ΔCd24a) by mouse peritoneal macrophages ($n = 5$ mice; unpaired, two-tailed Student's *t*-test with multiple comparisons correction, $^{*}P = 0.0196$). **b**, Representative bioluminescence image of tumour burden in C57Bl/6 mice with ID8 wild-type versus ID8(ΔCd24a) tumours (image taken 49 days after engraftment and representative of one experimental replicate). **c**, Burden of ID8 wild-type tumours (blue) versus ID8(ΔCd24a) tumours (red) as measured by bioluminescence imaging (WT, $n = 5$; ΔCd24a, $n = 5$; two-way ANOVA with multiple comparisons correction, tumour genotype $F_{(1,48)} = 10.70$, $^{***}P = 0.0001$). Data are representative of one experimental replicate. **d**, Extended measurement (as in Fig. 4e) of burden of MCF-7 wild-type tumours treated with IgG control (blue) versus anti-CD24 mAb (red) as measured by bioluminescence (IgG control, $n = 5$; anti-CD24 mAb, $n = 5$; days on which treatment was administered are indicated by arrows below the *x* axis; data are of one experimental cohort; two-way ANOVA with multiple comparisons correction, tumour treatment $F_{(1,81)} = 16.75$). $^{****}P < 0.0001$. Data are mean ± s.e.m.

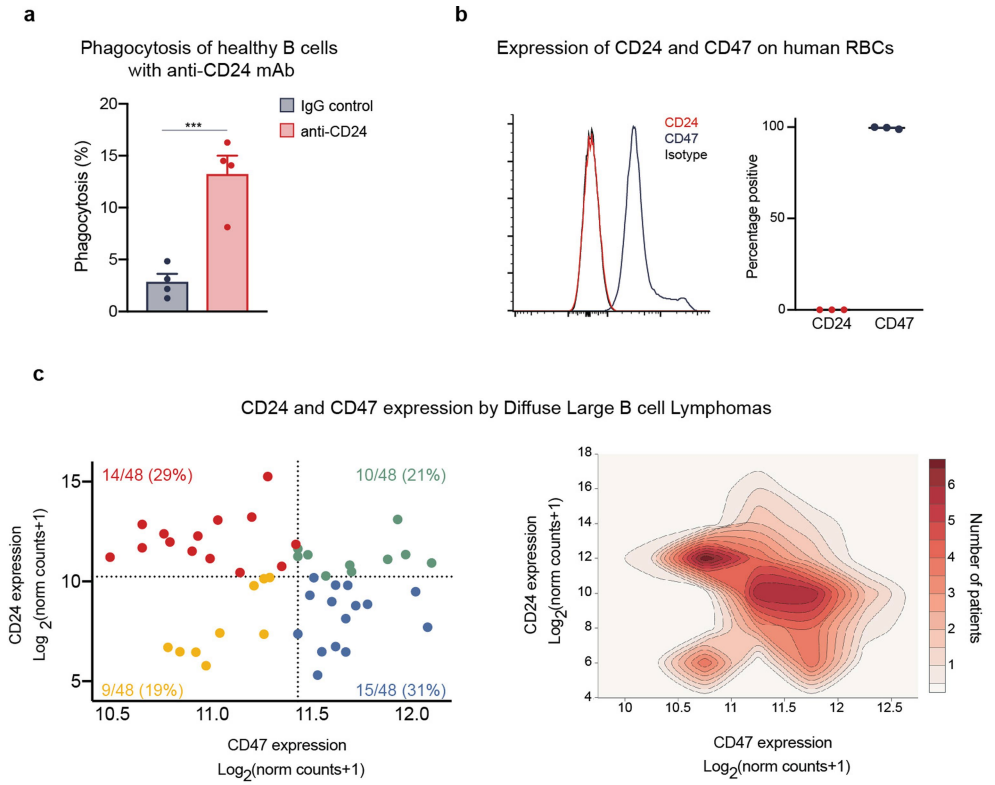

Extended Data Fig. 10 | Anti-CD24 mAb induces B cell clearance but does not bind human red blood cells, and CD47 and CD24 demonstrate inversely correlated expression in human diffuse large B-cell lymphoma. a, Flow-cytometry-based measurement of phagocytosis of B cells ($n = 4$ donors, pooled) by donor-derived macrophages ($n = 4$ donors) in the presence of anti-CD24 mAb as compared to IgG control; each symbol represents an individual donor (paired, two-tailed Student's *t*-test, $^{***}P = 0.0008$). **b**, Left, representative flow cytometry histogram measuring the expression of CD24 (red line) and CD47 (blue line) by human red blood cells (RBCs); right, flow-cytometry-based measurement of the frequency of $CD24^+$ compared with $CD47^+$ RBCs out of total RBCs ($n = 3$ donors). Data are mean ± s.e.m. **c**, Left, expression levels in $\log_2$(normalized counts + 1) of *CD24* and *CD47* in diffuse large B cell lymphomas from TCGA ($n = 48$); data are divided into quadrants by median expression of each gene as indicated by dotted lines. The number and percentage of total patients in each quadrant are indicated on the plot. Each dot indicates a single patient. Right, two-dimensional contour plot of expression levels of *CD24* and *CD47* in the large B cell lymphoma samples featured in the left plot.

nature research

Corresponding author(s): Irving L. Weissman

Last updated by author(s): Jun 13, 2019

Reporting Summary

Nature Research wishes to improve the reproducibility of the work that we publish. This form provides structure for consistency and transparency in reporting. For further information on Nature Research policies, see Authors & Referees and the Editorial Policy Checklist .

Statistics

For all statistical analyses, confirm that the following items are present in the figure legend, table legend, main text, or Methods section.

n/a	Confirmed	
☐	☒	The exact sample size (*n*) for each experimental group/condition, given as a discrete number and unit of measurement
☐	☒	A statement on whether measurements were taken from distinct samples or whether the same sample was measured repeatedly
☐	☒	The statistical test(s) used AND whether they are one- or two-sided *Only common tests should be described solely by name; describe more complex techniques in the Methods section.*
☐	☒	A description of all covariates tested
☐	☒	A description of any assumptions or corrections, such as tests of normality and adjustment for multiple comparisons
☐	☒	A full description of the statistical parameters including central tendency (e.g. means) or other basic estimates (e.g. regression coefficient) AND variation (e.g. standard deviation) or associated estimates of uncertainty (e.g. confidence intervals)
☐	☒	For null hypothesis testing, the test statistic (e.g. *F*, *t*, *r*) with confidence intervals, effect sizes, degrees of freedom and *P* value noted *Give P values as exact values whenever suitable.*
☒	☐	For Bayesian analysis, information on the choice of priors and Markov chain Monte Carlo settings
☒	☐	For hierarchical and complex designs, identification of the appropriate level for tests and full reporting of outcomes
☐	☒	Estimates of effect sizes (e.g. Cohen's *d*, Pearson's *r*), indicating how they were calculated

Our web collection on statistics for biologists contains articles on many of the points above.

Software and code

Policy information about availability of computer code

Data collection	Flow cytometry data was collected using FACSDiva 8.0.1 (BD). Bioluminescence data was collected using Living Image 4.2.
Data analysis	Flow cytometry data was analyzed using FACSDiva 8.0.1 (BD) and FlowJo 10 (Tree Star). Bioluminescence data was analyzed using Living Image 4.2. All graphs were generated and analyzed using GraphPad Prism 8. Indel analysis for gene knockouts was performed using TIDE 2.0.1. Single-cell RNA sequencing analysis was performed with STAR 2.5.3a. Contour plots were generated using Plotly 2018.

For manuscripts utilizing custom algorithms or software that are central to the research but not yet described in published literature, software must be made available to editors/reviewers. We strongly encourage code deposition in a community repository (e.g. GitHub). See the Nature Research guidelines for submitting code & software for further information.

Data

Policy information about availability of data

All manuscripts must include a data availability statement. This statement should provide the following information, where applicable:

- Accession codes, unique identifiers, or web links for publicly available datasets
- A list of figures that have associated raw data
- A description of any restrictions on data availability

All primary data for all figures and supplementary figures are available from the corresponding authors upon request.

Field-specific reporting

Please select the one below that is the best fit for your research. If you are not sure, read the appropriate sections before making your selection.

Life sciences study design

All studies must disclose on these points even when the disclosure is negative.

Sample size	Sample sizes were modeled after those from existing publications regarding in vitro immune killing assays and in vivo tumor growth assays, and an independent statistical method was not used to determine sample size. In our experience with in vitro measurements of phagocytosis, we have found that assaying human macrophages from 3 donors is sufficient for studies of antibody efficacy based off of observed variability among donors.
Data exclusions	As listed in the Methods, phagocytosis assays were performed in a minimum of technical triplicate for a minimum of 3 human donors per treatment group. In some cases, donors or specific technical replicates were excluded on the pre-established criterion that they were found to be a significant outlier by the GraphPad Outlier Calculator (https://www.graphpad.com/quickcalcs/Grubbs1.cfm). In some cases, additional replicates of specific phagocytosis assay conditions were repeated as part of pilot experiments, or as confirmatory replicates, but only a discrete set of data performed under identical conditions was specifically reported. For in vivo experiments, individual mice were removed from the study either prior to treatment, if found to be an engraftment outlier by bioluminescence imaging, or from the final analysis if, at end point, the mouse was found to be a significant outlier with regards to tumor growth. These exclusion criteria were established prior to tumor engraftment. All outlier calculations for in vivo experiments were performed using the GraphPad Outlier Calculator (https://www.graphpad.com/quickcalcs/Grubbs1.cfm). In some cases across additional experiments, including pilot experiments, additional mice were engrafted subcutaneously with relevant cell lines and followed for non-standard periods of time, or assessed for tumor growth at non-standard intervals, but only a discrete set of mice assessed under identical conditions was reported.
Replication	In vitro phagocytosis assays were performed in technical triplicate for a minimum of 3 human donors per treatment group with similar results and responses observed across donors and replicates. In vitro phagocytosis assays were performed across multiple experimental replicates, when possible, with the exceptions of the phagocytosis assays shown in Figure 2d (4 biological replicates, one experimental replicate), Figure 2g (4 biological replicates, one experimental replicate), Figure 2b (U-87 only; 3 biological replicates, one experimental replicate), Extended Data Figure 2e (3 biological replicates, one experimental replicate), Extended Data Figure 3c (4 biological replicates, one experimental replicate), Extended Data Figure 5c (3 biological replicates, one experimental replicate), Extended Data Figure 5d,f (4 biological replicates, one experimental replicate), Extended Data Figure 9a (4 biological replicates, one experimental replicate). Staining and recombinant Siglec binding experiments were performed in at least 2 experimental replicates. Automated live cell microscopy experiments were performed across at least technical and biological duplicates. Whenever practical for in vivo experiments, multiple cohorts across experimental replicates were performed. The number of cohorts performed is listed in the figure legends pertinent for each in vivo experiment. We observed similar results across cohorts and across individual mice within each cohort, as represented in the figures.
Randomization	For macrophage depletion experiments, mice pre-treated with either vehicle or anti-CSF1R mAb were randomized amongst treatment cohorts prior to engraftment with WT or CD24 KO MCF-7 tumors. Similarly, mice engrafted with MCF-7 tumors were randomized prior to treatment with anti-human CD24 mAb.
Blinding	All experiments, including in vivo experiments, were performed by unblinded investigators as all experiments in this work contained internal controls to allow for quantification and data analysis.

Reporting for specific materials, systems and methods

We require information from authors about some types of materials, experimental systems and methods used in many studies. Here, indicate whether each material, system or method listed is relevant to your study. If you are not sure if a list item applies to your research, read the appropriate section before selecting a response.

Materials & experimental systems

n/a	Involved in the study
[ ]	[x] Antibodies
[ ]	[x] Eukaryotic cell lines
[x]	[ ] Palaeontology
[ ]	[x] Animals and other organisms
[ ]	[x] Human research participants
[x]	[ ] Clinical data

Methods

n/a	Involved in the study
[x]	[ ] ChIP-seq
[ ]	[x] Flow cytometry
[x]	[ ] MRI-based neuroimaging

Antibodies

Antibodies used	All antibodies used in this work, clone, application, and supplier are listed in Supplementary Table 1.
Validation	The anti-human CD24 antibody (Clone SN3, Novus Bio (NB100-64861) and Creative Biolabs (CSC-S170)) used for staining and treatment studies in this work was validated by Novus Bio in human peripheral blood granulocytes. This antibody was also validated by staining unmodified MCF-7 cells versus CD24 knockout MCF-7 cells (dilution assessed in this work 1:50). The SN3

antibody was confirmed to not bind to mouse CD24a-expressing ID8 cells by flow cytometry. The CD24a antibody (Clone M1/69, BioLegend (101814)) was validated by staining unmodified ID8 cells versus CD24a knockout ID8 cells (dilution assessed in this work 1:100). The anti-human CD47 antibody used for treatments (Clone 5F9-G4, in house) is a clinical trial-grade humanized antibody which was validated as described in Liu et al. nature research | reporting summary October 2018 PLoS One (2015). The anti-human CD47 antibody used for staining (Clone B6H12, eBioscience (17-0479-42)) was validated by Barkal et al. Nature Immunology (2018) by comparing staining (dilution assessed in this work 1:100) of unmodified versus CD47 knockout cells. The Siglec-10 antibody (Clone 5G6, Thermo Scientific (MA5-28236)) has been validated by Thermo Fisher Scientific by staining CHO cells modified to express human Siglec-10 (dilution assessed in this work 1:50). The anti-human CD45 antibody (Clone HI30, BioLegend (304008)), the anti-human CD56 antibody (Clone HCD56, BioLegend (318316)), the anti-human CD3 antibody (Clone UCHT1, BioLegend (300415)), and the anti-human CD19 antibody (Clone SJ25C1, BioLegend (363011)) were all validated by the manufacturer by staining human peripheral lymphocytes (dilution assessed in this work 1:100). The anti-human/mouse CD11b antibody (Clone M1/70, BioLegend (101220)) was validated by the manufacturer by staining C57BL/6 mouse bone marrow cells (dilution assessed in this work 1:100). The anti-human CD14 antibody (Clone M5E2, BioLegend (301819)) was validated by the manufacturer by staining human peripheral blood monocytes (dilution assessed in this work 1:100). The anti-human EpCAM antibody (Clone 9C4, BioLegend (324204)) and the anti-human EpCAM antibody (Clone VU-1D9, ThermoFisher Scientific (BMS171)) were validated by the manufacturer by staining the HT29 human colon carcinoma cell line (dilution assessed in this work 1:100). The anti-human Siglec-5 antibody (Clone 1A5, BioLegend (352003)) was validated by the manufacturer by staining human peripheral blood granulocytes. The anti-human Siglec-9 antibody (Clone K8, BioLegend (351503)) was validated by the manufacturer by staining human peripheral blood monocytes. The anti-mouse CD45 antibody (Clone 30-F11, BioLegend (103106)) was validated by the manufacturer by staining C57BL/6 mouse splenocytes (dilution assessed in this work 1:100). The anti-mouse CD80 antibody (Clone 16-10A1, BioLegend (104725)) and the anti-mouse F4/80 antibody (Clone BM8, BioLegend (123114)) were validated by the manufacturer by staining thioglycolate-induced Balb/c mouse peritoneal macrophages (dilution assessed in this work 1:100). The anti-mouse CSF1R antibody (Clone AFS98, BioXCell (BE0213)) was validated by the investigators through FACS measurements of the frequency of tissue resident macrophages after 18 days of IP treatment with CSF1R antibody as compared to vehicle-treated mice.

Eukaryotic cell lines

Policy information about cell lines

Cell line source(s)	All cell lines used in this work were obtained from ATCC, with the exception of the APL1 human pancreatic neuroendocrine tumor line which was derived from a primary patient tumor as described in Krampitz et al. PNAS (2016) and the ID8 murine ovarian carcinoma cell line which was a gift from the laboratory of O. Dorigo.
Authentication	Cell lines were not independently authenticated beyond the identity provided from ATCC. The APL1 cell line was not independently authenticated beyond that performed in Krampitz et al. PNAS (2016). The ID8 murine ovarian carcinoma cell line was not independently authenticated.
Mycoplasma contamination	Stocks of all cell lines were tested for mycoplasma contamination prior to submission. All were negative.
Commonly misidentified lines (See ICLAC register)	None of the cell lines used in this study are listed in the database of commonly misidentified cell lines.

Animals and other organisms

Policy information about studies involving animals; ARRIVE guidelines recommended for reporting animal research

Laboratory animals	Animals used in xenograft experiments were 6-10 week old females of the NOD-scid IL2rγ-null (NSG) background obtained from in house breeding stocks. Animals used for syngeneic experiments were 6-8 week old females of the C57BL/6 background obtained from the Jackson Laboratory.
Wild animals	This study did not involve wild animals.
Field-collected samples	This study did not involve samples collected in the field.
Ethics oversight	All experiments were carried out in accordance with ethical care guidelines set by the Stanford University Administrative Panel on Laboratory Animal Care. Specific protocol numbers available on request.

Note that full information on the approval of the study protocol must also be provided in the manuscript.

Human research participants

Policy information about studies involving human research participants

Population characteristics	The primary human samples used in this work were all collected from female patients who had been diagnosed with ovarian cancer or breast cancer and who were operated on at Stanford University Medical Center. All patients were above 30 years of age and female. Information not protected by HIPAA (i.e. age, genotypic/molecular information) available on request.
Recruitment	Female patients with ovarian cancer and breast cancer identified by the surgeons (I. Wapnir, breast cancer; O. Dorigo, ovarian cancer; Human Immune Monitoring Center Biobank and Stanford Tissue Bank; breast cancer) were recruited for the IRB approved studies reported here.

Ethics oversight	The Human Immune Monitoring Center Biobank, the Stanford Tissue Bank, and Dr. Oliver Dorigo all received IRB approval from the Stanford University Administrative Panels on Human Subjects Research and complied with all ethical guidelines for human subjects research to obtain patient samples of ovarian cancer and breast cancer, and received informed consent from all patients. Specific IRB protocol numbers are available on request.

Note that full information on the approval of the study protocol must also be provided in the manuscript.

Flow Cytometry

Plots

Confirm that:

☒ The axis labels state the marker and fluorochrome used (e.g. CD4-FITC).

☒ The axis scales are clearly visible. Include numbers along axes only for bottom left plot of group (a 'group' is an analysis of identical markers).

☒ All plots are contour plots with outliers or pseudocolor plots.

☒ A numerical value for number of cells or percentage (with statistics) is provided.

Methodology

Sample preparation	Please also see description of sample preparation included in the Methods. Briefly: FACS of primary human tumors/mouse tumors: Solid tumors were excised and mechanically dissociated using a straight razor prior to incubation with 10 mL RPMI supplemented with 10 mL of RPMI + 10 µg/mL DNaseI (Sigma Aldrich) + 25 µg/mL Liberase (Roche) for 30-60 min at 37°C. Single cell suspensions were blocked using species-matched anti-CD16/32 antibodies (TruStain fcX, BioLegend) for 10 minutes on ice prior to staining. Gates were set by fluorescence minus one controls for markers other than CD24 and Siglec-10 which were set based off of isotype controls. All samples were analyzed while in FACS buffer containing 1 µg/mL DAPI in order to exclude dead cells. Channel compensations were performed using single-stained UltraComp eBeads (Affymetrix) or cells. In vitro phagocytosis assay: All phagocytosis assay wells were stained with anti-human/mouse CD11b antibody (Clone M1/70, BioLegend) for 30 minutes on ice, prior to analysis. All samples were analyzed while in FACS buffer containing 1 µg/mL DAPI in order to exclude dead cells. Gates were set based off of fluorescence minus one controls. Data was analyzed using FlowJo (Treestar) and outliers among technical replicates in each treatment group were removed using GraphPad Outlier Calculator (http://graphpad.com/quickcalcs/Grubbs1.cfm).
Instrument	All samples were analyzed on an LSR Fortessa (BD) or Aria II SORP (BD).
Software	FACS data was collected using FACS Diva (BD) and analyzed using FACS Diva (BD) or FlowJo (Tree Star). Statistical analyses and plots were generated using GraphPad Prism 8.
Cell population abundance	The CD24-null MCF7-7 and ID8 CD24a-null cell lines were sorted based off of positive controls (WT versions of each cell line). After the initial knockout was performed, the CD24-null cell lines approximately 10% of the population, while in successive purification sorts, the CD24-null population was >70% of the population. No other populations were sorted for this manuscript.
Gating strategy	All gating strategies used in this work are included in the Extended Data Figures. Briefly: FACS of primary human tumors: The frequency of CD24+ cancer cells was measured as the number of DAPI–CD14–EpCAM+CD24+ cells out of total DAPI–CD14–EpCAM+ cells as determined by isotype controls. The frequency of Siglec-10+ TAMs was measured as the number of DAPI–EpCAM–CD14+CD11b+Siglec-10+ cells out of total DAPI–EpCAM–CD14+CD11b+ cells, as determined by isotype controls (Gating Strategy Extended Data Figure 2a). In vitro phagocytosis assays: Phagocytosis was defined as the frequency of the DAPI-CD11b+GFP+ population among all DAPI-CD11b+ cells (Gating Strategy Extended Data Figure 3). In vivo TAM phagocytosis assays: In vivo phagocytosis was defined as the DAPI-CD45+ CD11b+F480+GFP+ population out of total TAMs defined as DAPI-CD45+ CD11b+F480+ cells (Gating Strategy Extended Data Figure 5a). M1-like mouse TAMs: The frequency of M1-like mouse TAMs was measured as DAPI–, CD45+, CD11b+, F480+, CD80+ TAMs out of total TAMs defined as DAPI-CD45+ CD11b+F480+, as defined by fluorescence minus one controls (Gating Strategy Extended Data Figure 5a).

☒ Tick this box to confirm that a figure exemplifying the gating strategy is provided in the Supplementary Information.